Review

Field-Theoretic Computer Simulation Methods for Polymers and Complex Fluids

Glenn H. Fredrickson,*,† Venkat Ganesan,‡,§ and François Drolet||

Mitsubishi Chemical Center for Advanced Materials and Departments of Chemical Engineering & Materials and Department of Chemical Engineering, University of California, Santa Barbara, California 93106-5080; and Hyperdigm Research, 102 De Gascogne, St-Lambert, QC J4S-1C8, Canada

Received August 22, 2001

ABSTRACT: We review a class of new computer simulation methods for polymeric fluids and other soft condensed matter systems that are based on an underlying field-theoretic description. These methods, while still in an early stage of development, show considerable promise for studying the equilibrium properties of many-component systems capable of intricate self-assembly, such as solutions and blends containing block and graft copolymers. Field-theoretic simulation methods also provide a great deal of flexibility in model building and coarse graining, and appear to be particularly well suited to treat systems with soft, long-range interactions, such as polyelectrolytes. We attempt to connect various related theoretical approaches, such as self-consistent field theory and dynamic density functional theory, within a common framework.

I. Introduction

Many practical applications of polymers and other soft condensed matter systems involve mixtures that through equilibrium self-assembly or nonequilibrium processing steps develop complex, multiphase morphologies. The desirable and marketable properties of such materials, which include plastic alloys, block and graft copolymers, and polyelectrolyte solutions, complexes, and gels, depend critically on the ability to control and manipulate morphology by adjusting a combination of molecular and macroscopic variables. For example, styrene−butadiene block copolymers can be devised that serve either as rigid, tough, and transparent thermoplastics or as soft, flexible, and thermoplastic elastomers, by appropriate control of copolymer architecture and styrene/butadiene ratio.[1] In this case, the property profiles are intimately connected to the relationship between the molecular parameters and the extent and type of nanoscale self-assembly that takes place within the materials. Unfortunately, such relationships are traditionally determined by trial and error experimentation that is both laborious and costly. In the design of new materials, it would obviously be highly desirable if theoretical methods could be used to anticipate nano- and microscale self-assembly and further relate such morphological characteristics to properties of interest in specific applications.

Unfortunately, theoretical techniques for anticipating the structure and equilibrium phase behavior of complex polymeric fluids are still in their infancy. Nonequilibrium methods for predicting structural evolution and properties of multiphase systems under realistic processing conditions are even less developed. Nevertheless, progress is being made and current theoretical tools have met with sufficient success to justify use in many of the R&D organizations of leading polymeric materials suppliers.

Modern computer simulation methods for polymers and other soft materials[2−13] can be grouped into three major categories: *atomistic*, *coarse-grained particle-based*, and *field-theoretic*. Fully atomistic methods typically involve building classical (as opposed to quantum) descriptions of a polymeric or complex fluid with atomic resolution. Interactions in such models are described by some combination of bonded and nonbonded potential functions, typically parametrized at the two-body and/or three-body level. In principle these potentials can be obtained by quantum chemical calculations, so that first principles parametrization of new systems is possible. Determination of equilibrium or nonequilibrium properties involves carrying out a computer simulation, usually by employing Monte Carlo (MC) or molecular dynamics (MD) techniques. The major drawback of atomistic methods is that, except in rare instances, it is very difficult to equilibrate sufficiently large systems of polymers at realistic densities in order to extract meaningful information about structure and thermo-

* Corresponding author. E-mail: ghf@mrl.ucsb.edu.
† Mitsubishi Chemical Center for Advanced Materials and Departments of Chemical Engineering & Materials, University of California, Santa Barbara.
‡ Department of Chemical Engineering, University of California, Santa Barbara.
§ Permanent address: Department of Chemical Engineering, University of Texas, Austin, TX 78712.
|| Hyperdigm Research.

10.1021/ma011515t CCC: $22.00
Published on Web 12/26/2001

dynamics. This limitation is particularly acute for multiphase, inhomogeneous systems, which are often those of primary interest.

A reasonable alternative to a fully atomistic computer simulation is a *coarse-grained, particle-based* approach[2] in which atoms or groups of atoms are lumped into larger "particles". At the lowest level this could simply amount to a "united atom" approach where, e.g., each CH_2 unit in a polyethylene chain is replaced by a single effective particle. Interactions in such a model are then effective interactions between lumped CH_2 particles and standard MC or MD simulation methods can be employed. Often even more extensive coarse graining is carried out. For example, bead-spring polymer chains are often employed in which each bead might represent the force center associated with 10 or more backbone atoms. A difficulty with such models is that the effective interactions between beads (particles) are often difficult to parametrize accurately. Moreover, they remain expensive to simulate, especially at melt densities and for heterogeneous systems that exhibit nanoscale or macroscale phase separation.[9,13] One solution to speed up the simulations is to introduce artificially soft repulsive interparticle potentials, as is conventionally done in dissipative particle dynamics (DPD),[14] but this has a number of adverse effects including artificially high fluid phase compressibilities, loss of topological constraints between chains, and often loss of connection to the atomic/chemical details of the underlying complex fluid.

In both of the above modeling strategies, the fundamental degrees of freedom to be sampled in a computer simulation are the generalized coordinates (including bond and torsional angles) associated with the atoms or particles. As we shall describe below, an alternative approach, at least for computing equilibrium properties, is to integrate out the particle coordinates in the partition function, replacing them instead with *functional integrals over one or more fluctuating chemical potential fields* that are confined to a simulation domain. In constructing such *field-theoretic models* it is often convenient from the start to smear the particle force centers uniformly along the polymer backbones, so that a discrete bead-spring chain model becomes a continuous chain described by a space curve $\mathbf{R}(s)$.[15]

Starting with Edwards,[16] field theory models have been extensively used as the basis for approximate analytical calculations on a variety of important systems including polymer solutions, melts, blends, and copolymers.[17−21] Until very recently, however, field-theory models have *not been the basis of a computer simulation strategy* for polymers or other soft condensed matter systems. This is particularly surprising given the rich history of lattice gauge simulation methods[22,23] applied to field theories in nuclear, high energy, and hard condensed matter physics. It is our belief that adaption and improvement of these "field-theoretic simulation" (FTS) methods to enable direct numerical sampling of field theory models of complex fluids (without approximation beyond numerical error) will provide a powerful suite of tools for exploring the equilibrium properties of a wide range of important soft materials systems. In the specific case of polymers, we anticipate that such "field-theoretic polymer simulation" (FTPS) methods[24] will be competitive with more conventional particle-based simulation methods, especially when applied to dense, multiphase systems with many components. Future development of the methods may also provide access to nonequilibrium properties.

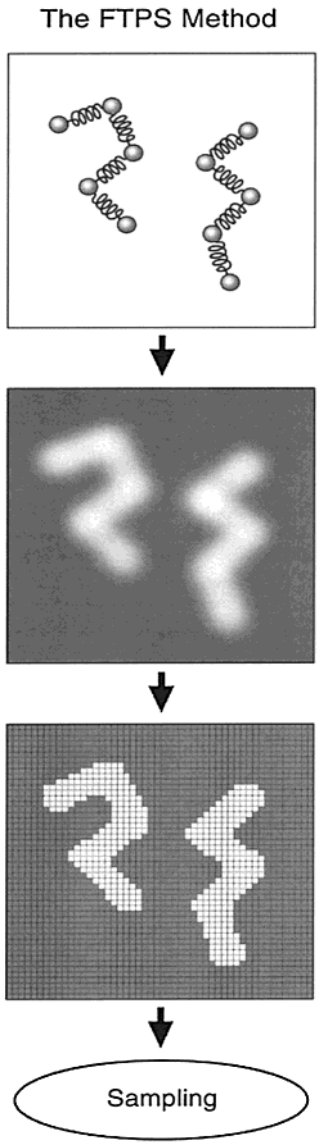

Figure 1. Summary of the "field-theoretic polymer simulation" (FTPS) method. In step 1 a microscopic model (atomistic or mesoscale) is constructed in which the degrees of freedom are $3n$ particle coordinates, $\mathbf{r}^n$, representing positions of monomers, solvents, solutes, etc. In step 2, the microscopic model is converted by formally exact methods to a field theory involving one or more chemical potential fields $w(\mathbf{r})$. Step 3 involves meshing the simulation domain to facilitate either a finite difference or finite element representation of the relevant fields. The degrees of freedom at this stage are the N_g components of the discretized chemical potential fields, corresponding to values of w on the nodes or lattice sites as appropriate. Step 4 involves a numerical procedure to sample states in this N_g-dimensional w-space with complex statistical weight $\sim \exp(-H[w^{N_g}])$.

In the present review, we survey this approach and attempt to unify and classify the various field-theoretic methods that are currently in use. While we have made no attempt to be comprehensive and have drawn heavily from our own work, we have tried to connect with ongoing activities in several of the leading research groups in the area. Nonetheless, we apologize in advance for our failure to cite all of the relevant and important literature.

Overall, the general FTS/FTPS strategy for calculating equilibrium properties involves four steps that are

depicted in Figure 1: (1) development of a suitable particle-based model, (2) conversion of the particle-based model into a field theory, (3) discretization of the simulation domain, and (4) numerical sampling of the discretized field theory. Step 1 requires some "art" because the starting model may either be atomistic or coarse-grained; moreover, steps 1 and 2 may be omitted in situations where the starting model is already a field theory. Step 2 is carried out by using exact analytical methods as described below. Step 3, like step 1, is highly flexible and can be accomplished by conventional finite difference or finite element representations of the fields. Alternatively, modern adaptive, unstructured finite element methods[25] could in principle be applied, or various spectral methods could be used. Step 4 will receive special attention in this review because we shall see that the discretized field theories relevant to simple and complex fluids have a nonpositive definite statistical weight, which would seem to rule out standard sampling methods such as Monte Carlo (MC). We argue that a complex Langevin dynamics (CLD)[26−28] method originally developed in the context of lattice gauge theory is a particularly convenient strategy for overcoming this difficulty.

The present review is organized as follows. In section II, we discuss the general strategy for building field-theoretic models and provide several examples in the context of simple monatomic fluids, polymer solutions, polymer blends, and block copolymers. This section addresses steps 1 and 2 above. Section III discusses the general mathematical structure of the field theories when extended to the complex plane and the representation of observables in the field-theoretic language. We shall see a close connection between saddle points of the field theories and a familiar mean-field theory known as self-consistent field theory (SCFT) that has been widely applied to polymers. Section IV discusses various implementations of SCFT, as well as a related mean-field theory known as dynamic density functional theory (DDFT). Section V then addresses how to go beyond the mean-field approximation and to implement full numerical sampling of a field theory model, i.e., to implement a FTPS. Finally, in section VI we provide our current thoughts on the advantages and limitations of the field-theoretic simulation methods, as well as discuss extensions and future developments.

II. Model Building

There are many possible approaches to building field theory models of soft materials that can be studied by the methods of this review. A fundamental starting point is an atomistic model that can be converted to a field theory by standard methods. We illustrate with a simple model of a classical monatomic fluid.

A. Monatomic Fluids. Consider a monatomic fluid in the canonical ensemble.[29] For a collection of n particles in a three-dimensional volume V, the $3n$-dimensional configurational phase space can be denoted by $\mathbf{r}^n = (\mathbf{r}_1, \mathbf{r}_2, ..., \mathbf{r}_n)$, where $\mathbf{r}_j$ is the position of the jth particle in the volume. If the potential energy can be pairwise decomposed, the configurational partition function can be written

$$Z = \int \mathrm{d}\mathbf{r}^n \exp(-(\beta/2)\sum_{j(\neq k)}\sum_{k} v(|\mathbf{r}_j - \mathbf{r}_k|)) \qquad (1)$$

where $v(r)$ is the familiar pair interaction potential. Subsequently we work in energy units where $\beta \equiv 1/(k_B T) = 1$. For cases in which the potential is singular at the origin, we regularize it by the replacement $v(r) \rightarrow v(r + \epsilon)$, and later take $\epsilon \rightarrow 0+$. Upon introduction of the microscopic particle density $\hat{\rho}(\mathbf{r}) = \sum_j \delta(\mathbf{r} - \mathbf{r}_j)$, the partition function can be rewritten as $Z = \int \mathrm{d}\mathbf{r}^n \exp[-U(\mathbf{r}^n)]$, where

$$U(\mathbf{r}^n) = \frac{1}{2}\int \mathrm{d}\mathbf{r} \int \mathrm{d}\mathbf{r}'\, \hat{\rho}(\mathbf{r}) v(|\mathbf{r} - \mathbf{r}'| + \epsilon)\hat{\rho}(\mathbf{r}') \qquad (2)$$

and we have ignored a configuration-independent, multiplicative factor of $\exp[nv(\epsilon)/2]$ in Z, which represents a constant shift in free energy due to particle self-interactions. In eq 2, we have expressed the potential energy as a quadratic form in the microscopic density; a more general fluid model with three-body potentials would contribute cubic terms in $\hat{\rho}$, etc.

Our next step is to insert a δ functional identity, namely $\int \mathscr{D}[\rho]\, \delta(\rho - \hat{\rho}) = 1$, in the integrand of the partition function, where $\int \mathscr{D}[\rho]$ denotes a functional integral over a real density field $\rho(\mathbf{r})$ defined within the volume V.[30] We then give the functional δ, which constrains the fields $\rho(\mathbf{r})$ and $\hat{\rho}(\mathbf{r})$ to be the same at each point $\mathbf{r}$, an exponential representation: $\delta(\rho - \hat{\rho}) = \int \mathscr{D}[w] \exp[i \int \mathrm{d}\mathbf{r}\, w(\rho - \hat{\rho})]$, where $i \equiv \sqrt{-1}$. This introduces a second functional integral over a *real* scalar field $w(\mathbf{r})$ that can be interpreted as a *fluctuating chemical potential field*. These two steps have the net effect of eliminating all particle−particle interactions—replacing them instead with interactions between individual particles and the fluctuating field w. As a result, the $\int \mathrm{d}\mathbf{r}_j$ coordinate integrals are the same for each particle j and factor, leading to

$$Z = \int \mathscr{D}[\rho] \int \mathscr{D}[w] \exp(-H[\rho, w]) \qquad (3)$$

where the "effective Hamiltonian" is given by

$$H[\rho, w] = \frac{1}{2}\int \mathrm{d}\mathbf{r} \int \mathrm{d}\mathbf{r}'\, \rho(\mathbf{r}) v(|\mathbf{r} - \mathbf{r}'| + \epsilon)\rho(\mathbf{r}') - i \int \mathrm{d}\mathbf{r}\, w\rho - n \ln Q[iw] \qquad (4)$$

and

$$Q[iw] = V^{-1} \int \mathrm{d}\mathbf{r} \exp[-iw(\mathbf{r})] \qquad (5)$$

is the partition function of a single particle in the purely imaginary potential $iw(\mathbf{r})$. In writing eq 3, we have again dropped configuration-independent terms such as V^n, which produce constant shifts in the free energy (in this case contributing to the ideal gas free energy). It is also understood that the limit $\epsilon \rightarrow 0+$ is to be taken at the end of any thermodynamic calculation.

Equations 3 and 4 constitute the field theory model that corresponds to the atomistic particle-based model of eq 1. With an eye toward computing equilibrium properties, the focus has changed from evaluating a $3n$-dimensional configurational integral over the particle coordinates to the problem of computing two *functional* integrals over density and chemical potential fields. There are two important differences between the potential energy function $U(\mathbf{r}^n)$ appearing in the original theory and the effective Hamiltonian functional $H[\rho, w]$ appearing in the corresponding field theory:

•$H[\rho, w]$ contains an entropy term $-n(\ln Q)$ and so has a "free energy" character, while U represents only potential energy.

•$H[\rho, w]$ is *complex*, implying a nonpositive definite statistical weight $\exp(-H)$; in contrast, U is purely real.

Both of these differences prove to be very important in the development of field-theoretic simulation methods. The second point deserves special mention. While H is complex and can be decomposed into real and imaginary parts according to $H = H_R + iH_I$, the fields ρ and w are real, as is the partition function Z. It follows that Z can alternatively be expressed as $Z = \int \mathcal{D}[\rho] \int \mathcal{D}[w] \exp(-H_R) \cos(H_I)$, where the integrand is explicitly real, but is *not positive definite*, due to the phase factor $\cos(H_I)$. This feature is also encountered in lattice gauge theories, where it is referred to as the "sign problem."[31] A final comment is that very similar steps can be followed to transform the partition functions of particle-based models in other ensembles, e.g., the grand canonical ensemble,[32] to suitable field theories. For simplicity, we discuss only the canonical ensemble in the present review.

In the most general case of potential energy functions U containing three-body or higher-order potentials, the functional $H[\rho, w]$ is not a quadratic form in ρ, so it is not possible to further simplify eq 3. However, if the interactions are pairwise and the potential v has only real, positive eigenvalues so that an inverse v^{-1} defined by $\int d\mathbf{r}'' \, v(|\mathbf{r} - \mathbf{r}''| + \epsilon)v^{-1}(|\mathbf{r}'' - \mathbf{r}'|,\epsilon) = \delta(\mathbf{r} - \mathbf{r}')$ exists, the Gaussian integral over ρ can be explicitly carried out. In this case eqs 3 and 4 simplify to $Z = \int \mathcal{D}[w] \exp(-H[w])$, with

$$H[w] = \frac{1}{2} \int d\mathbf{r} \int d\mathbf{r}' \, w(\mathbf{r}) v^{-1}(|\mathbf{r} - \mathbf{r}'|,\epsilon) w(\mathbf{r}') - n \ln Q[iw] \quad (6)$$

and where we again discard normalizing factors in Z. This last step cannot be performed for many realistic potentials that are harshly repulsive at short distances (e.g., the Lennard-Jones 6−12 potential). However, the simplification does apply for several important cases including the Coulomb potential, the Yukawa (or Debye−Huckel) potential, and a repulsive δ function pseudo-potential, $v(r) = u_0\delta(\mathbf{r})$, $u_0 > 0$.

B. Homopolymer Solutions. Having demonstrated how an atomistic model of a simple fluid can be converted to a field theory, we now turn to consider the development of models for homopolymer solutions. It is apparent that one approach would be to simply retrace the steps of the previous section, starting with a fully atomistic model of both polymers and solvent. However, frequently one is primarily concerned with polymer solution structure and thermodynamics associated with length scales much larger than atomic dimensions, in which case a better starting point is to treat the solvent as a continuum and employ a coarse-grained polymer model. For the case of *flexible polymers*, a convenient choice of chain model is the "Gaussian thread model," which corresponds to the continuum limit of harmonic bead-spring chains as described earlier. In this model, polymers are represented by continuous space curves $\mathbf{R}_\alpha(s)$, where $\alpha = 1, ..., n$ indexes the different polymers and s is an arc length variable running from 0 to 1 along each chain contour.[15] We again consider a canonical ensemble in which n polymers are confined to a volume V. Conformations of noninteracting polymers are given a Gaussian statistical weight, $\exp(-U_0)$, with a harmonic stretching (free) energy given by (units of k_BT):

$$U_0[\mathbf{R}] = \frac{1}{4R_{g0}^2} \sum_{\alpha=1}^{n} \int_0^1 ds \left| \frac{d\mathbf{R}_\alpha(s)}{ds} \right|^2 \quad (7)$$

The quantity R_{g0} is the unperturbed radius-of-gyration of a chain, $R_{g0}^2 = Nb^2/(2d)$, where b is the statistical segment length, N is the polymerization index, and d is the space dimension ($d = 3$ in three dimensions).

Nonbonded interactions of mean force between monomers on the same polymer and between monomers on different polymers, in both cases mediated by the solvent, are typically represented by a pairwise pseudopotential.[15] The appropriate energy function $U_1[\mathbf{R}]$ is obtained from eq 2 by the replacement $v(r) \rightarrow u_0\delta(\mathbf{r})$. The microscopic monomer density in this case is defined by $\hat{\rho}(\mathbf{r}) = N\sum_\alpha \int_0^1 ds \, \delta(\mathbf{r} - \mathbf{R}_\alpha(s))$. Under good solvent conditions, $u_0 > 0$, pair interactions are sufficient; for poor solvents, $u_0 < 0$, a stabilizing three-body potential term is required.

Because the δ function pair potential is invertible for the case of good solvents, it is possible to retrace the steps of the last section and transform the starting microscopic model defined by $Z = \int \mathcal{D}[\mathbf{R}] \exp(-U_0 - U_1)$ to an equivalent field theory involving a single fluctuating chemical potential field, $Z = \int \mathcal{D}[w] \exp(-H[w])$. The notation $\int \mathcal{D}[\mathbf{R}]$ denotes n path integrals over all possible space curves describing the conformations of the chains. The effective Hamiltonian of the resulting field theory reduces to (for $\epsilon \rightarrow 0+$)

$$H[w] = \frac{1}{2u_0} \int d\mathbf{r} \, w^2 - n \ln Q[iw] \quad (8)$$

where $Q[iw]$ is now interpreted as the *partition function of a single polymer* in the purely imaginary potential $iw(\mathbf{r})$.

The evaluation of Q is more complicated for flexible polymers than for point particles, cf. eq 5. Formally, we can express Q as a path integral[17,33]

$$Q[iw] = \frac{\int \mathcal{D}[\mathbf{R}] \exp[-U_0 - iN \int_0^1 ds \, w(\mathbf{R}(s))]}{\int \mathcal{D}[\mathbf{R}] \exp[-U_0]} \quad (9)$$

where only one polymer chain need be considered. The normalization is the same as in eq 5, i.e., $Q[0] = 1$. A convenient way to evaluate this path integral is to express it in terms of a restricted partition function $q(\mathbf{r}, s;[w])$ that satisfies a complex diffusion equation. (We will subsequently drop the functional dependence on w to simplify the notation.) This equation is analogous to the Feynman−Kac formula familiar in the path integral description of quantum mechanics.[34] In particular, $q(\mathbf{r}, s)$ is obtained as the solution of the equation

$$\frac{\partial}{\partial s} q(\mathbf{r}, s) = R_{g0}^2 \nabla^2 q(\mathbf{r}, s) - iNw(\mathbf{r}) q(\mathbf{r}, s) \quad (10)$$

subject to the "initial condition" $q(\mathbf{r}, 0) = 1$. The single-chain partition function, which can be viewed as a functional of the field $w(\mathbf{r})$, is computed by integrating eq 10 forward along the chain contour from $s = 0$ to $s = 1$ and then performing a volume average:

$$Q[iw] = \frac{1}{V}\int \mathrm{d}\mathbf{r}\; q(\mathbf{r}, 1) \tag{11}$$

The structure of eqs 10 and 11 implies that for general $w(\mathbf{r})$, both $q(\mathbf{r}, s)$ and Q are complex quantities.

In summary, for a simple microscopic model of flexible polymers in a good solvent, the partition function can be transformed into a field theory of the form $Z = \int \mathscr{D}[w] \exp(-H[w])$, where the effective Hamiltonian is defined by eqs 8, 10, and 11. By expressing all lengths in units of R_{g0} and introducing a rescaled potential field, $W(\mathbf{r}) \equiv Nw(\mathbf{r})$, it is apparent that all intensive thermodynamic properties of the model can be expressed in terms of just *two* parameters:

$$C = nR_{g0}{}^d/V,\; B = u_0N^2/R_{g0}{}^d \tag{12}$$

The first parameter C is a dimensionless polymer concentration, while the second $B \sim N^{(4-d)/2}$ is a dimensionless excluded volume parameter that is encountered in perturbation theories of the excluded volume effect. This field theory has been known for many years to be a good starting point for approximate analytical calculations at various values of B, $C > 0$ that traverse the dilute, semidilute and concentrated polymer solution regimes.[15,16,19−21] To our knowledge, however, this field theory model has *not been previously viewed as the basis for a computer simulation method*. For completeness, we summarize the model equations in dimensionless form:

$$Z = \int \mathscr{D}[W] \exp(-H[W]) \tag{13}$$

$$H[W] = \frac{1}{2B}\int \mathrm{d}\mathbf{r}\; W^2 - CL^d \ln Q[iW] \tag{14}$$

$$Q[iW] = \frac{1}{L^d}\int \mathrm{d}\mathbf{r}\; q(\mathbf{r}, 1) \tag{15}$$

$$\frac{\partial}{\partial s} q(\mathbf{r}, s) = \nabla^2 q(\mathbf{r}, s) - iW(\mathbf{r})q(\mathbf{r}, s), \quad q(\mathbf{r}, 0) = 1 \tag{16}$$

In the above, L denotes the length of the system in units of R_{g0}, i.e., $L^d \equiv V/R_{g0}{}^d$.

Our overall philosophy on model building is that one should start with the simplest possible model that captures the essence of molecular structure and interactions for a system of interest, and add more details only if warranted by comparison with experiment. For example, the two-parameter model outlined above provides a satisfactory model of many solutions of flexible polymers in good solvents. At least one more parameter is required, however, to describe flexible polymers in theta or poor solvents.[35] For *semi-flexible* polymer solutions, the wormlike chain model (Kratky−Porod model)[36] is often more appropriate than the Gaussian thread model of eq 8. In this case, a diffusion equation approach to computing Q is also available. A tendency for nematic ordering can be incorporated by adding an anisotropic Maier−Saupe or Onsager-type interaction term to the overall potential energy of the model.[37] Finally, it is also possible to build field theory models of polymer solutions that reflect more atomic-level detail of polymer, solvent, or the interactions between the two. For example, the rotational isomeric state (RIS) model[38] can be substituted for either the Gaussian thread or wormlike chain model, in which case transfer matrix methods could be used in place of diffusion equations to compute the single-chain partition function. It is also possible to evaluate the functional Q by Monte Carlo or other *stochastic* simulation methods,[39] although such an approach is computationally very expensive relative to the *deterministic* methods of computing Q described here.

C. Polymer Blends and Block Copolymers. Having discussed the description of polymer solutions, we now turn to heterogeneous melts of flexible polymers. For simplicity, we focus on two cases: (i) a binary blend of a type A homopolymer with a second type B homopolymer and (ii) an AB diblock copolymer melt. Again, if one is interested primarily in mesoscale and macroscale structure and thermodynamics, a coarse-grained starting point is appropriate. A typical model[17] invokes the Gaussian thread model to describe the *bonded interactions* for both A and B species, e.g., for a *binary polymer blend*

$$U_0[\mathbf{R}_A,\mathbf{R}_B] = \frac{1}{4R_{g0,A}{}^2}\sum_{\alpha=1}^{n_A}\int_0^1 \mathrm{d}s\,\left|\frac{\mathrm{d}\mathbf{R}_{\alpha A}(s)}{\mathrm{d}s}\right|^2 + \frac{1}{4R_{g0,B}{}^2}\sum_{\alpha=1}^{n_B}\int_0^1 \mathrm{d}s\,\left|\frac{\mathrm{d}\mathbf{R}_{\alpha B}(s)}{\mathrm{d}s}\right|^2 \tag{17}$$

where $\mathbf{R}_{\alpha K}(s)$ denotes the space curve describing the conformations of the αth type-K chain, n_K is the number of chains of species K (A or B), and $R_{g0,K} = b_K[N_K/(2d)]^{1/2}$ is the unperturbed radius-of-gyration of a type-K chain. The *nonbonded interactions* can again be expressed in terms of microscopic monomer densities defined by $\hat{\rho}_K(\mathbf{r}) = N_K\sum_{\alpha=1}^{n_K}\int_0{}^1\mathrm{d}s\;\delta(\mathbf{r} - \mathbf{R}_{\alpha K}(s))$. There are two types of nonbonded interactions that are important to capture. The first is the tendency for a preference of similar (A−A and B−B) binary monomer contacts over dissimilar (A−B) contacts in a blend, which arises primarily from *attractive* (cohesive) intermonomer forces. This tendency can be described by a simple quadratic form

$$U_1[\mathbf{R}_A,\mathbf{R}_B] = v_0\chi\int \mathrm{d}\mathbf{r}\;\hat{\rho}_A\hat{\rho}_B \tag{18}$$

familiar in regular solution (and Flory−Huggins) theory, where χ is the Flory parameter.[35] We have conveniently defined monomers (statistical segments) so that they occupy the same volume in the melt, i.e., $v_A = v_B \equiv v_0$. The total average monomer density is given by $\rho_0 \equiv 1/v_0 = (n_AN_A + n_BN_B)/V \equiv \rho_{A0} + \rho_{B0}$.

The second type of nonbonded interactions that are important to capture in a model of polymer melts are the *harshly repulsive* ("hard core") interactions that lead to small variations in total monomer density on meso- and macroscales. A simple way to incorporate such interactions is through a strict "incompressible melt" approximation, which is imposed by a functional δ, $\delta(\hat{\rho}_A + \hat{\rho}_B - \rho_0)$, that forces the sum of the two microscopic densities, $\hat{\rho}_A(\mathbf{r}) + \hat{\rho}_B(\mathbf{r})$, to be equal to the average total density ρ_0 at each point $\mathbf{r}$ in the system. Assembling all three types of interactions produces the following "microscopic" model of a molten binary polymer blend:

$$Z = \int \mathscr{D}[\mathbf{R}_A]\int \mathscr{D}[\mathbf{R}_B]\;\delta(\hat{\rho}_A + \hat{\rho}_B - \rho_0)\times \exp(-U_0 - U_1) \tag{19}$$

Our final task is to convert this model involving $n_A + n_B$ chain conformation path integrals into a field theory where the fundamental degrees of freedom are fluctuating chemical potential fields. To this end, it is convenient to express the microscopic densities appearing in Z in terms of the linear combination fields

$$\hat{\rho}_{\pm}(\mathbf{r}) \equiv \hat{\rho}_A(\mathbf{r}) \pm \hat{\rho}_B(\mathbf{r}) \tag{20}$$

Because of the δ function constraint on the plus field, $\hat{\rho}_+(\mathbf{r}) = \rho_0$, the interaction term U_1 can be rewritten as

$$U_1[\mathbf{R}_A,\mathbf{R}_B] = -\nu_0\chi/4 \int d\mathbf{r}\, [\hat{\rho}_-(\mathbf{r}) - (\rho_{A0} - \rho_{B0})]^2 \tag{21}$$

where we have made a constant shift in the free energy by adding (configuration independent) terms that are zeroth and first order in the $\hat{\rho}_-$ field. The next step is to introduce two real, fluctuating chemical potential fields, $w_-(\mathbf{r})$ and $w_+(\mathbf{r})$, which serve, respectively, to decouple the quadratic $\hat{\rho}_-$ interactions manifest in U_1 and to give the δ functional an exponential representation:

$$\exp(-U_1) = \int \mathscr{D}[w_-] \exp\Big(\int d\mathbf{r}\, [(\hat{\rho}_- - \rho_{A0} + \rho_{B0})w_- - 1/(\chi\nu_0)w_-^2]\Big) \tag{22}$$

$$\delta(\hat{\rho}_+ - \rho_0) = \int \mathscr{D}[w_+] \exp(-i \int d\mathbf{r}\, w_+[\hat{\rho}_+ - \rho_0]) \tag{23}$$

The field w_- is a type of "exchange chemical potential", since it appears conjugate to the density difference $\hat{\rho}_-$. In contrast, w_+ is a total chemical potential, or "pressure," that is conjugate to the total monomer density $\hat{\rho}_+$ and enforces incompressibility.

Collecting the above results, one can reexpress eq 19 as a field theory in the two real chemical potential fields $w_\pm$

$$Z = \int \mathscr{D}[w_+] \int \mathscr{D}[w_-] \exp(-H[w_+, w_-]) \tag{24}$$

where

$$H[w_+, w_-] = \int d\mathbf{r}\, [(\rho_{A0} - \rho_{B0})w_- - i\rho_0 w_+ + \rho_0\chi^{-1}w_-^2] - n_A \ln Q_A[iw_+ - w_-] - n_B \ln Q_B[iw_+ + w_-] \tag{25}$$

The functionals $Q_K[\psi_K]$ (K = A or B) represent the partition functions of a single type-K polymer in a (generally complex) chemical potential field $\psi_K(\mathbf{r})$. These can be obtained by the same strategy as in the previous section; i.e., $Q_K[\psi_K] = V^{-1} \int d\mathbf{r}\, q_K(\mathbf{r}, 1)$, where $q_K(\mathbf{r}, s)$ satisfies

$$\frac{\partial}{\partial s} q_K(\mathbf{r}, s) = R_{g0,K}^2 \nabla^2 q_K(\mathbf{r}, s) - N_K \psi_K(\mathbf{r}) q_K(\mathbf{r}, s) \tag{26}$$

subject to the initial condition $q_K(\mathbf{r}, 0) = 1$.

Apart from the linear terms in the $w_\pm$ fields, which have no thermodynamic significance, the above field theory for an incompressible binary polymer blend is quite similar in structure to those derived previously for monatomic fluids (eq 6) and polymer solutions (eq 8). In the present case we see that the "pressure" field w_+ is most similar to the w fields introduced previously—all are conjugate to the total monomer/atom density. Moreover, we see that the effective Hamiltonian $H[w_+, w_-]$ acquires an *imaginary* part due to the pressure field w_+, which is a manifestation of the *repulsive* interactions. In contrast, the *attractive* interactions are decoupled by an exchange potential w_- that makes *real* contributions to H. In general, because realistic models of fluids always contain repulsive interactions, the sampling problem associated with a complex effective Hamiltonian (described in detail in section V) cannot be avoided.

It is straightforward to adapt the above model to describe an *incompressible melt of AB diblock copolymers*.[40] In the simplest version, we ignore differences in statistical segment length between the two blocks, $b_A = b_B \equiv b$, and consider n diblock molecules of total polymerization index N in a volume V. The volume fraction of type A segments on each molecule is denoted f and coincides with the global volume fraction of type A segments: $f = \rho_{A0}/\rho_0$. By following the same steps as above, it can be shown that the partition function for such a model can be written in the form of eq 24, but with a slightly modified version of the effective Hamiltonian:

$$H[w_+, w_-] = \int d\mathbf{r}\, [\rho_0(2f - 1)w_- - i\rho_0 w_+ + \rho_0\chi^{-1}w_-^2] - n \ln Q[iw_+ - w_-, iw_+ + w_-] \tag{27}$$

In this expression, $Q[\psi_A,\psi_B]$ is the partition function of a single diblock copolymer experiencing a (complex) chemical potential field $\psi_A(\mathbf{r})$ acting on the type A monomers and a complex field $\psi_B(\mathbf{r})$ acting on the type B monomers.

Before writing an explicit expression for Q in the case of a diblock melt, it is convenient to implement the scalings applied previously in the polymer solution case—namely, we express all lengths in units of the unperturbed overall copolymer radius-of-gyration, R_{g0}, and rescale the fields according to $W_\pm \equiv Nw_\pm$. This leads to the following dimensionless field theory model for an incompressible diblock copolymer melt

$$Z = \int \mathscr{D}[W_+] \int \mathscr{D}[W_-] \exp(-H[W_+, W_-]) \tag{28}$$

where

$$H[W_+, W_-] = C \int d\mathbf{r}\, [(2f - 1)W_- - iW_+ + 1/(\chi N)W_-^2] - CL^d \ln Q[iW_+ - W_-, iW_+ + W_-] \tag{29}$$

and $C = nR_{g0}^d/V$ is the dimensionless chain concentration introduced earlier. The single-chain partition function can be expressed as $Q[iW_+ - W_-, iW_+ + W_-] = L^{-d} \int d\mathbf{r}\, q(\mathbf{r}, 1)$, where $q(\mathbf{r}, s)$ satisfies

$$\frac{\partial}{\partial s} q(\mathbf{r}, s) = \nabla^2 q(\mathbf{r}, s) - \psi(\mathbf{r}, s) q(\mathbf{r}, s) \tag{30}$$

subject to $q(\mathbf{r}, 0) = 1$ and with

$$\psi(\mathbf{r}, s) \equiv \begin{cases} iW_+(\mathbf{r}) - W_-(\mathrm{r}), & 0 < s < f \\ iW_+(\mathbf{r}) + W_-(r), & f < s < 1 \end{cases} \tag{31}$$

This completes the field-theoretic description of an incompressible AB diblock copolymer melt. We note that the model involves *four dimensionless* parameters: the chain concentration C, an effective strength of repulsion between the A and B blocks χN, the copolymer composition f, and the system size L. The intensive thermodynamic quantities of a bulk system depend only on the first three parameters. Because the parameter C mul-

tiplies all terms in the effective Hamiltonian H, we shall see that it plays a special role in the theory.

Clearly, similar methods can be used to construct field theory models of much more complicated polymer blends with arbitrary numbers of components, and with components that are themselves copolymers. Models of more complicated block, graft, and star copolymers are also straightforward to build. Charged species can be incorporated to create models of electrolytes, polyelectrolytes, and block and graft co-polyelectrolytes.[41,42] It is also possible to develop models with chemical disorder in the form of chain length polydispersity or sequence disorder (statistical copolymers).[43,44] Finally, one can combine different chain models (e.g., wormlike chains and Gaussian thread chains) to create field-theoretic descriptions of systems such as rod−coil block copolymers, liquid crystalline side-chain polymers and copolymers, etc.[45]

III. Field Theory Models: General Features and Observables

In the above sections we have provided several examples of how field theory models of simple and complex fluids (including polymers) can be constructed. It is now appropriate to discuss some general features of these models and describe how to formally obtain expressions for physical observables of interest.

A. Observables. It is convenient to work in the context of the *polymer solution model* and examine how thermodynamic averages of various physically significant quantities are calculated. As will be described in a subsequent section, FTS simulations involve numerical sampling of chemical potential field configurations, i.e., the W field for polymer solutions, with field configurations assigned a statistical weight proportional to $\exp(-H[W])$ Thus, to compute ensemble averages of physical observables in such a scheme, it is necessary to make explicit the functional dependence of these quantities on the field W.

We begin by considering monomer density correlation functions. For this purpose, it is convenient to generalize the polymer solution model to include a source term $\mu(\mathbf{r})$:[30]

$$Z[\mu] = \int \mathscr{D}[\mathbf{R}] \exp(-\mathrm{U}_0 - \mathrm{U}_1 - \int \mathrm{d}\mathbf{r}\, \mu\hat{\rho}) \quad (32)$$

Clearly the original partition function is given by $Z = Z[0]$. However, density correlation functions can be generated by taking functional derivatives with respect to μ. For example

$$\langle\hat{\rho}(\mathbf{r})\rangle = -\left.\frac{\delta \ln Z[\mu]}{\delta\mu(\mathbf{r})}\right|_{\mu=0} \quad (33)$$

and

$$\langle\hat{\rho}(\mathbf{r})\hat{\rho}(\mathbf{r}')\rangle - \langle\hat{\rho}(\mathbf{r})\rangle\langle\hat{\rho}(\mathbf{r}')\rangle = \left.\frac{\delta^2 \ln Z[\mu]}{\delta\mu(\mathbf{r})\,\delta\mu(\mathbf{r}')}\right|_{\mu=0} \quad (34)$$

The averages denoted $\langle ... \rangle$ on the left-hand side of eq 34 represent equilibrium ensemble averages with respect to the $\mathbf{R}(s)$ variables and with the Boltzmann statistical weight $\exp(-U_0 - U_1)$ of the starting model. If we transform eq 32 into a form analogous to eq 8, it follows that the average density can be expressed as

$$\langle\hat{\rho}(\mathbf{r})\rangle = -n\left\langle\left.\frac{\delta \ln Q[iw+\mu]}{\delta\mu(\mathbf{r})}\right|_{\mu=0}\right\rangle = in\left\langle\frac{\delta \ln Q[iw]}{\delta w(\mathbf{r})}\right\rangle \quad (35)$$

The averages on the right-hand side of these two expressions now denote equilibrium ensemble averages with respect to the w field, i.e., $\langle(...)\rangle \equiv Z^{-1}\int \mathscr{D}[w] \exp(-H[w])(...)$, with $H[w]$ given in eq 8. It follows that we can define a *complex monomer density operator*

$$\rho(\mathbf{r};[w]) \equiv in\frac{\delta \ln Q[iw]}{\delta w(\mathbf{r})} \quad (36)$$

such that the average monomer density is given by $\langle\hat{\rho}(\mathbf{r})\rangle = \langle\rho(\mathbf{r};[w])\rangle$. For a particular (real) w field configuration, the density operator $\rho(\mathbf{r};[w])$ is *complex*; in contrast, the average density is purely real. For a bulk homogeneous polymer solution, evidently the equilibrium average monomer density is given by $\langle\rho(\mathbf{r};[w])\rangle \equiv \rho_0 = nN/V$.

It is clear from eq 36 that the monomer density operator can be computed strictly from knowledge of the single chain partition function $Q[iw]$. By invoking a well-known factorization property of the single chain path integral,[17,33,34] it is possible to rewrite the right-hand side of eq 36 in terms of the restricted partition function already encountered in eq 10

$$\rho(\mathbf{r};[w]) = \frac{\rho_0}{Q}\int_0^1 \mathrm{d}s\; q(\mathbf{r}, s)q(\mathbf{r}, 1-s) \quad (37)$$

For practical computations of the density operator $\rho(\mathbf{r};[w])$, it is convenient to decompose both ρ and q into real and imaginary parts, e.g., $q = q_\mathrm{R} + iq_\mathrm{I}$. Given some potential field $w(\mathbf{r})$, eq 10 is decomposed into two real diffusion equations for q_R and q_I, which are integrated forward in s, starting from $q_\mathrm{R}(\mathbf{r}, 0) = 1$, $q_\mathrm{I}(\mathbf{r}, 0) = 0$. These solutions are then inserted into eq 37 and numerical quadratures performed to approximate the s integral and obtain the real and imaginary parts of the density operator.

Similar formulas can be derived for pair correlation functions of the monomer density. However, instantaneous values (at one particular w field configuration) of second order correlation functions require a fundamental (point source) solution of the diffusion equation, which is rather expensive to compute. Fortunately, ensemble averages of complex correlation function operators (representing the observables) can be easily obtained by constructing appropriate correlation functions of $w(\mathbf{r})$. Specifically, using eq 8 and eq 36, the average density can be written

$$\langle\rho(\mathbf{r};[w])\rangle = \frac{i}{Z}\int \mathscr{D}[w] \exp\left[-\frac{1}{2u_0}\int \mathrm{d}r\; w^2\right]\frac{\delta}{\delta w(\mathbf{r})} \times \exp(n \ln Q[iw]) \quad (38)$$

Integrating this equation by parts (assuming the boundary terms can be neglected) yields

$$\langle\rho(\mathbf{r};[w])\rangle = -\frac{i}{Z}\int \mathscr{D}[w] \exp(n \ln Q[iw])\frac{\delta}{\delta w(\mathbf{r})} \times \exp\left[-\frac{1}{2u_0}\int \mathrm{d}\mathbf{r}\; w^2\right] = \frac{i}{u_0}\langle w(\mathbf{r})\rangle \quad (39)$$

which provides an alternative expression for the first

moment of the monomer density. (Note that $\langle w(\mathbf{r})\rangle$ turns out to be pure imaginary.) In a similar manner, one can derive an expression for the two point density correlation function. Explicitly, we utilize the identity

$$\int \mathscr{D}[w]\, A[w] \frac{\delta^2}{\delta w^2} B[w] = -\int \mathscr{D}[w] \frac{\delta}{\delta w} A[w] \frac{\delta}{\delta w} B[w] = \int \mathscr{D}[w]\, B[w] \frac{\delta^2}{\delta w^2} A[w] \quad (40)$$

where $A[w]$ and $B[w]$ are arbitrary functionals (provided the boundary terms vanish). The choice $A = \exp[-1/(2u_0) \int d\mathbf{r}\, w^2]$ and $B = \exp(n \ln Q[iw])$ can be used to derive the following expression for the monomer density pair correlation function:

$$\langle \hat{\rho}(\mathbf{r})\hat{\rho}(\mathbf{r}')\rangle - \langle \hat{\rho}(\mathbf{r})\rangle \langle \hat{\rho}(\mathbf{r}')\rangle = \frac{1}{u_0}\delta(\mathbf{r}-\mathbf{r}') - \frac{1}{u_0^2}[\langle w(\mathbf{r})w(\mathbf{r}')\rangle - \langle w(\mathbf{r})\rangle\langle w(\mathbf{r}')\rangle] \quad (41)$$

The first term proportional to $\delta(\mathbf{r} - \mathbf{r}')$ is a spurious monomer self-interaction term that is normally discarded.

Next we turn to consider the *osmotic pressure* of a polymer solution in the field-theoretic framework. The thermodynamic definition of the osmotic pressure is $\pi \equiv -\partial F/\partial V)_{n,T}$,[15] where F is the Helmholtz free energy. By explicitly forming this derivative in the starting polymer solution model, it is possible to derive an expression closely related to the "virial equation" from liquid state theory:[29]

$$\beta\pi = n/V + \frac{1}{V}\langle U_1\rangle - \frac{2}{3V}(\langle U_0\rangle - \langle U_0\rangle_0) \quad (42)$$

In this expression, we have restored the "ideal gas" term n/V corresponding to the infinite dilution limit of noninteracting polymers ($u_0 = 0$) and employed the notation $\langle(...)\rangle_0$, denoting an ensemble average with statistical weight $\exp(-U_0)$. Upon introduction of the reduced variables of the polymer solution model and a dimensionless osmotic pressure $\Pi \equiv \beta\pi R_{g0}{}^d$, we find

$$\Pi = C - \frac{1}{2BL^d}\int d\mathbf{r}\, \langle W^2(\mathbf{r})\rangle + \frac{2}{3}C\left\langle \frac{P[iW]}{Q[iW]}\right\rangle \quad (43)$$

where now all averages on the right hand side denote ensemble averages over W field fluctuations. The functional $P[iW]$ can be expressed as $P[iW] = L^{-d} \int d\mathbf{r}\, p(\mathbf{r}, 1)$, where $p(\mathbf{r}, s)$ satisfies

$$\frac{\partial}{\partial s}p(\mathbf{r}, s) = \nabla^2[p(\mathbf{r}, s) - q(\mathbf{r}, s)] - iW(\mathbf{r})p(\mathbf{r}, s), \quad p(\mathbf{r}, 0) = 0 \quad (44)$$

The above examples for the polymer solution model have illustrated how density correlation functions and the osmotic pressure can be related to the W field configurations that are directly sampled in a field-theoretic simulation. It is straightforward to generalize these connections to cover a broader range of physical observables, to properties in other ensembles such as the grand canonical and isothermal−isobaric, and to other models of polymers and complex fluids. While we avoid further elaboration of such formulas here, it is convenient to present the generalization of the density operator formula eq 37 for the case of the *incompressible AB diblock copolymer model*. Specifically, we introduce a (complex) reduced species density operator (K = A or B), $\phi_K(\mathbf{r};[W_\pm]) \equiv \rho_K(\mathbf{r};[W_\pm])/\rho_0$, whose ensemble average over the $W_\pm$ field configurations is the (real) *average volume fraction* of species K:

$$\phi_K(\mathbf{r}) = \langle \phi_K(\mathbf{r};[W_\pm])\rangle \quad (45)$$

The volume fraction operators are obtained from a composition formula similar to eq 37. Because diblock copolymers are not symmetric with respect to interchange of the two ends, however, the factorization of the copolymer path integral introduces a second restricted partition function $q^\dagger(\mathbf{r}, s;[W_\pm])$.[40] In the functional q, s is the contour distance measured from the free end of the A block, while in $q^\dagger$, s is measured away from the free end of the B block. [Despite the misleading (conventional) notation, $q^\dagger$ is a distinct functional from q and does not represent the Hermitian conjugate of q. Both are complex quantities.] The composition formulas are as follows:

$$\phi_A(\mathbf{r};[W_\pm]) = \frac{1}{Q}\int_0^f ds\, q(\mathbf{r}, s)\, q^\dagger(\mathbf{r}, 1-s) \quad (46)$$

$$\phi_B(\mathbf{r};[W_\pm]) = \frac{1}{Q}\int_f^1 ds\, q(\mathbf{r}, s)\, q^\dagger(\mathbf{r}, 1-s) \quad (47)$$

The auxiliary functional $q^\dagger$ satisfies

$$\frac{\partial}{\partial s} q^\dagger(\mathbf{r}, s) = \nabla^2 q^\dagger(\mathbf{r}, s) - \psi^\dagger(\mathbf{r}, s)\, q^\dagger(\mathbf{r}, s) \quad (48)$$

subject to $q^\dagger(\mathbf{r}, 0) = 1$ and with

$$\psi^\dagger(\mathbf{r}, s) \equiv \begin{cases} iW_+(\mathbf{r}) + W_-(\mathbf{r}), & 0 < s < 1-f \\ iW_+(\mathbf{r}) - W_-(\mathbf{r}), & 1-f < s < 1 \end{cases} \quad (49)$$

B. Saddle Points. A very important characteristic of the models described in the above sections is the identification of *stationary field configurations* that correspond to extrema of the complex effective Hamiltonian H.[30] For a real field theory, such a configuration can be a local minimum, maximum, or a saddle point in the field configuration space. However, when the field variables are extended to the complex plane, the energy surface is generally saddle shaped in the vicinity of an extremum, so we shall refer to stationary field configurations as *saddle points*.

For the *polymer solution model* described by eq 14, saddle point field configurations, denoted $W^*(\mathbf{r})$, are obtained from

$$\left.\frac{\delta H[W]}{\delta W(\mathbf{r})}\right|_{W^*} = 0 \quad (50)$$

Considering the explicit form of eq 14 and noting the definition of the complex density operator in eq 36 leads to the following saddle point equation:

$$W^*(\mathbf{r})/B + iC\rho(\mathbf{r};[W^*])/\rho_0 = 0 \quad (51)$$

This equation has a *unique, homogeneous solution* $W^* = -iBC$ that lies on the negative imaginary axis (note $B, C > 0$) in the complex W plane.

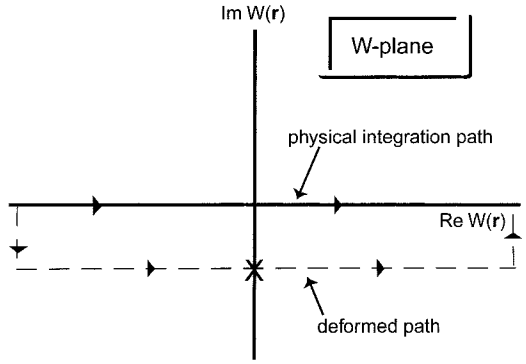

Figure 2. Complex plane for the $W(\mathbf{r})$ field in the polymer solution model at a fixed value of $\mathbf{r}$. The physical path of integration in the starting model is along the real axis. By deforming the path of integration onto the dashed path that passes through the saddle point (denoted by "×"), and is locally a constant phase path, it is possible to carry out a steepest-descent evaluation of the partition function. At leading order, such a procedure recovers mean-field theory.

The significance of the saddle point W^* is that it represents a *mean-field approximation* to the polymer solution model of eq 13. This connection between saddle points and mean field theory is textbook material in field theory and condensed matter physics,[30] and it has been known for quite some time in the polymer physics literature.[17,46] To explain the connection for the polymer solution model, we refer to Figure 2, which depicts the complex plane for the chemical potential field $W(\mathbf{r})$ at some fixed position $\mathbf{r}$ within the volume L^d. Because W was introduced as a real field, the path of integration in eq 13 is along the real W axis in Figure 2. We refer to this path as the "physical path of integration." The saddle point, denoted by an "×", lies on the negative imaginary axis. Because the integrand of eq 13 is analytic in W (note that $\exp(n \ln Q[iw]) = Q[iw]^n$, where n is an integer), we can invoke Cauchy's theorem to deform the path of integration from the physical path onto the dashed "deformed path" in Figure 2 that passes through the saddle point. This deformation can be accomplished by the simple shift of field to $\tilde{W}(\mathbf{r}) = W(\mathbf{r}) + iBC$, which transforms the polymer solution model into

$$Z = \exp(-H[W^*]) \int \mathscr{D}[\tilde{W}] \exp(-\tilde{H}[\tilde{W}]) \qquad (52)$$

$$\tilde{H}[\tilde{W}] = \frac{1}{2B} \int \mathrm{d}\mathbf{r}\ \tilde{W}^2 - iC \int \mathrm{d}\mathbf{r}\ \tilde{W} - CL^d \ln Q[i\tilde{W}] \qquad (53)$$

The integral on $\tilde{W}$ is now along the real axis and the saddle point lies at the origin. If we decompose $\tilde{H}[\tilde{W}]$ into real and imaginary parts according to $\tilde{H} = \tilde{H}_R + i\tilde{H}_I$ and expand about the origin to quadratic order in $\tilde{W}$, it is possible to show that $\tilde{H}_R = \int \mathrm{d}\mathbf{r} \int \mathrm{d}\mathbf{r}'\ K(\mathbf{r},\mathbf{r}') \tilde{W}(\mathbf{r})\tilde{W}(\mathbf{r}') + O(\tilde{W}^4)$ and $\tilde{H}_I = O(\tilde{W}^3)$, where $K(\mathbf{r},\mathbf{r}')$ is a real, symmetric, positive definite kernel. This demonstrates that, to quadratic order about the saddle point, the deformed path of integration is a *constant phase path* (i.e., $\tilde{H}_I$ is constant) and that $\tilde{H}_R$ has a *local minimum* along the deformed path at the saddle point.

The purpose of the above discussion has been to argue that, in this simple case of the polymer solution model, it is possible to deform the path of integration so that the saddle point configuration of the chemical potential field lies on a constant phase (or steepest) path of the functional integral defining the partition function. Because C appears as a prefactor in the nontrivial terms of eq 53, the method of steepest descent[47] can thus be used to carry out an asymptotic analysis of the partition function for $C \to \infty$. To leading order, it follows that

$$Z \approx Z_0 \exp(-H_R[W^*]) = Z_0 \exp(-L^d BC^2/2), \quad C \to \infty \qquad (54)$$

where H_R denotes the real part of H, and we have restored the previously neglected multiplicative prefactors through a factor of Z_0, representing the partition function of an "ideal gas" of noninteracting polymers. It follows that the saddle point configuration of the field recovers the familiar *mean-field approximation* for the excess Helmholtz free energy $F - F_0 = -\ln(Z/Z_0)$:[15]

$$F - F_0 \approx H_R[W^*] = \frac{1}{2} L^d BC^2 \qquad (55)$$

Our method of deriving the mean-field approximation also makes clear the fact that it is the leading term in an asymptotic expansion of $F - F_0$ for $C \to \infty$.

We have just demonstrated in the context of the polymer solution model an explicit connection between the saddle point chemical potential field configuration of the model and a corresponding mean-field approximation to the free energy. This proves to be a *general feature* of statistical field theory models.[17,30,46] The polymer solution model is particularly simple in that it possesses only a single saddle point, $W^* = -iBC$, which is homogeneous and located on the imaginary axis in the W-plane. Other models can possess multiple saddle points, both homogeneous and inhomogeneous, and can be located at arbitrary positions in the relevant field-plane. For example, a simple fluid with a purely repulsive Yukawa potential, $v(r) = (a/r) \exp(-\kappa r)$, a, $\kappa > 0$, which can be described by the field theory of eq 6, has a number of saddle points. It can be shown for this model that all saddle points are located on the *imaginary* axis of the w-plane and that a distinct saddle point exists for each possible thermodynamic phase of the system. In particular, the repulsive Yukawa model has a *homogeneous* saddle point corresponding to the fluid phase (liquid and gas are indistinguishable), with much the same character as the saddle point of the polymer solution model discussed above. This saddle point represents a mean-field approximation to the thermodynamic properties of the fluid phase. The repulsive Yukawa model, however, also possesses a number of *inhomogeneous* saddle points describing mean-field approximations for various crystal phases. In three dimensions, saddle points with simple cubic (sc), body-centered-cubic (bcc), and face-centered-cubic (fcc) symmetries (as well as others) in principle all exist for the model. If we order these saddle points according to the corresponding real parts of $H[w]$ (for a specific temperature, density, and set of model parameters), i.e., $H_R[w_1^*] < H_R[w_2^*] < H_R[w_3^*]$ ..., then clearly saddle point 1 represents a *stable* equilibrium crystal, while saddle points 2, 3, ... are *metastable or unstable* for the prescribed conditions, at least within the mean-field approximation.

The AB diblock copolymer model described in section II.C is another interesting case. The model is formulated in terms of two fields, W_+ and W_-, that were introduced to decouple repulsive and attractive interactions, respectively. Saddle points correspond to solutions of

$$\left.\frac{\delta H[W_+, W_-]}{\delta W_+(\mathbf{r})}\right|_{W_\pm^*} = 0, \left.\frac{\delta H[W_+, W_-]}{\delta W_-(\mathbf{r})}\right|_{W_\pm^*} = 0 \quad (56)$$

which are actually a set of *four* equations, since H is complex. It is possible to show that all saddle points of the model, both homogeneous and inhomogeneous, have W_+^* located on the imaginary axis and W_-^* purely real. A single homogeneous saddle point exists—representing a mean-field approximation for the *disordered phase* of a diblock copolymer melt. As shown in Figure 3, this disordered phase saddle point is located at the origin, $W_+^* = W_-^* = 0$, which is a consequence of the various shifts in free energy that we made in formulating the model. It follows that the reference state of free energy, F_0, is the disordered phase in the mean-field approximation. The various *ordered mesophases*, e.g., lamellar, hexagonal cylindrical, and bcc spherical phases, can be associated with distinct inhomogeneous saddle points having the appropriate crystallographic symmetries. Each of these inhomogeneous saddle points represent mean-field solutions of the model that can be characterized as stable, metastable, or unstable, just as in the repulsive Yukawa system.

For the diblock copolymer model as formulated, the physical path of integration is along the real axis in both the complex W_+ and W_- planes. As shown in Figure 3 for the W_+ plane, the disordered phase saddle point lies along this path at the origin. For small values of the parameter χN, this is the thermodynamically relevant saddle point (i.e., it is associated with the smallest value of H_R), and the path of integration can be shown to be a constant phase path to quadratic order near the origin. The parameter C is clearly relevant to controlling the accuracy of the mean-field approximation, since it multiplies all terms in the effective Hamiltonian of the model, eq 29. Thus, we can again invoke the steepest-descent method to argue that the excess Helmholtz free energy is given asymptotically for large C by $F - F_0 \approx H_R[W_+^*, W_-^*] = H_R[0, 0] = 0$, recovering the mean-field approximation.[17] Fluctuation corrections, important for smaller values of C, can be investigated by systematically extending the asymptotic expansion to include higher order terms. At larger values of χN, the disordered phase saddle point becomes metastable or unstable, and one of the *inhomogeneous* saddle points in Figure 3 dominates the functional integral defining the partition function. In principle, it is then possible to identify a deformed path (dashed path in Figure 3) that passes through the relevant saddle point (e.g., LAM in Figure 3) on a trajectory that is locally a constant phase path. This would permit formal justification of the mean-field approximation as being asymptotically exact for $C \rightarrow \infty$ and provide a steepest-descent framework for developing finite-C fluctuation corrections to the thermodynamic properties of the inhomogeneous mesophases of the model. Unfortunately, the identification of an appropriate deformed path of integration in the complex $W_\pm$ planes for arbitrary values of the model parameters χN and f turns out to be nontrivial. We will return to discuss this point further when we address sampling techniques in a later section.

It is important to emphasize that in the case of polymer models, it is well-known that *mean-field solutions corresponding to inhomogeneous saddle points are identical to those obtained using a theory known as self-consistent field theory* (SCFT).[17,46−49] This theory has been widely applied in the analysis of the excluded volume effect, polymer brushes, block copolymer mesophases, polymer blends and emulsions, and polymer−polymer interfaces and in many other situations where inhomogeneous polymeric phases are present. Indeed, we will show in the next section that the saddle point conditions, eq 56, can be directly reduced to the familiar SCFT equations for a diblock copolymer melt.[40]

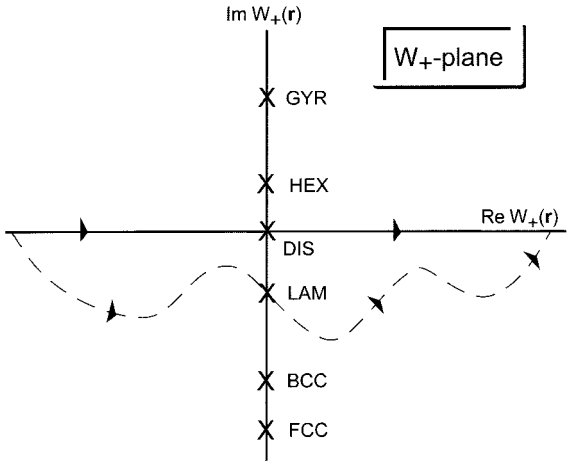

Figure 3. Complex plane for the $W_+(\mathbf{r})$ field in the AB diblock copolymer model at a fixed value of $\mathbf{r}$. The physical path of integration in the starting model is along the real axis, which passes through the disordered phase (homogeneous) saddle point denoted DIS. The model also possesses inhomogeneous saddle points located along the imaginary W_+ axis that have the symmetry of the various copolymer mesophases, including LAM (lamellar), HEX (cylindrical), BCC (spherical), and GYR (gyroid). By deforming the path of integration onto a dashed path that passes through an inhomogeneous saddle point (e.g., LAM shown), and that is locally a constant phase path, it is possible to carry out a steepest-descent evaluation of the partition function for an ordered mesophase. At leading order, such a procedure recovers mean-field theory.

In summary, SCFT is an *approximate* mean-field theory that can be viewed as a saddle point approximation to a field theory model of a polymer or complex fluid. Indeed, it is useful to classify numerical algorithms for implementing SCFT as algorithms for finding saddle points. This will be the subject of the next section.

IV. Finding Saddle Points: Implementation of SCFT

A. General Issues. When confronted with a new field theory model of a polymer or complex fluid, an important first step is to locate and classify the saddle points of the theory. By comparing values of H_R for a full set of saddle points and tracking how these change with the parameters of the model, it is possible to construct a phase diagram in the mean-field approximation. This amounts to an implementation of SCFT. Besides the obvious benefit of a mean-field solution, we shall see that a global understanding of the location of saddle points in the complex plane and the local behavior of the complex functional H in their vicinity is key to implementing field-theoretic simulation (FTS/FTPS) methods. In the case of homogeneous saddle points, such as the saddle point of the polymer solution model, analytical methods can generally be applied. Numerical methods are usually required to locate inhomogeneous saddle points.

The task of computing inhomogeneous saddle points can be viewed as a type of *nonlinear optimization*

problem: specifically, what are the chemical potential field configurations in the complex plane for which the effective Hamiltonian is stationary? Associated with such problems are a number of important issues:

1. How does one find all the relevant saddle points of a model?
2. How does one locate the most thermodynamically significant saddle points, i.e., those with the smallest values of H_R?
3. How does one accomplish 1 and 2 in the most computationally efficient manner?

In item 1 we note that an *uncountable* number of inhomogeneous saddle points can often be associated with continuous translations or rotations ("Goldstone modes"), or with topological defects in an unbounded periodic structure. Normally, however, there are a finite number of saddle points that differ in energy and are not related by simple rotations or translations and that are defect free. These are considered to be the "relevant" saddle points. Unfortunately, there appears to be no definitive theoretical answer to any of the above questions. Nevertheless, the field of nonlinear optimization is quite advanced and many practical numerical strategies have been devised.[50,51] The application of these methods to field theory models of polymers and complex fluids is in its infancy, however, so much room exists for improvements in the strategy and numerical implementation of SCFT.

Before discussing particular techniques for finding inhomogeneous saddle points, it is helpful to make use of some of the general features of the field theory models that were described in section III. For this purpose we consider the model of an incompressible AB diblock copolymer melt summarized by eqs 28−31. The saddle point equations for this model are given in eq 56 and because of the complex nature of H, represent a set of four real equations. We first consider the two equations associated with $\delta H/\delta W_+$. Explicitly forming this derivative leads to

$$\frac{\delta H[W_+, W_-]}{\delta W_+(\mathbf{r})} = iC[\phi_A(\mathbf{r};[W_\pm]) + \phi_B(\mathbf{r};[W_\pm]) - 1] \quad (57)$$

where the ϕ_K are the complex reduced monomer density operators defined by eqs 46−47 and we have made use of a formula similar to eq 36. It follows that the first complex equation in 56 corresponds to the following two real equations:

$$\mathrm{Re}\left[\frac{\delta H[W_+, W_-]}{\delta W_+(\mathbf{r})}\right]_{W^*_\pm} = -\phi_{A,I}(\mathbf{r};[W^*_\pm]) - \phi_{B,I}(\mathbf{r};[W^*_\pm]) = 0 \quad (58)$$

$$\mathrm{Im}\left[\frac{\delta H[W_+, W_-]}{\delta W_+(\mathbf{r})}\right]_{W^*_\pm} = \phi_{A,R}(\mathbf{r};[W^*_\pm]) + \phi_{B,R}(\mathbf{r};[W^*_\pm]) - 1 = 0 \quad (59)$$

where we again employ subscripts R and I, respectively, to denote the real (Re) and imaginary (Im) parts of a complex quantity. Because the parameter C appears as a prefactor in H, it drops out of the saddle point equations. Thus, the intensive thermodynamic properties of an incompressible block copolymer melt in mean-field theory depend on only two parameters: f and χN. Repeating the same procedure for the second complex equation in 56 leads to

$$\mathrm{Re}\left[\frac{\delta H[W_+, W_-]}{\delta W_-(\mathbf{r})}\right]_{W^*_\pm} = 2f - 1 - \phi_{A,R}(\mathbf{r};[W^*_\pm]) + \phi_{B,R}(\mathbf{r};[W^*_\pm]) + (2/\chi N)W^*_{-,R} = 0 \quad (60)$$

$$\mathrm{Im}\left[\frac{\delta H[W_+, W_-]}{\delta W_-(\mathbf{r})}\right]_{W^*_\pm} = -\phi_{A,I}(\mathbf{r};[W^*_\pm]) + \phi_{B,I}(\mathbf{r};[W^*_\pm]) + (2/\chi N)W^*_{-,I} = 0 \quad (61)$$

At this point, the four coupled equations 58−61 are simply an explicit expansion of the content of eqs 56. While these are sufficient to solve for the four field components ($W^*_{+,R}$, $W^*_{+,I}$, $W^*_{-,R}$, $W^*_{-,I}$) (subject to suitable boundary conditions), we can invoke our general understanding of the location of the saddle points to reduce the computational effort in half. Specifically, we expect saddle point solutions for W^*_+ to be *purely imaginary*, because that field is associated with the *repulsive* interactions of the model, while W^*_- is associated with the *attractive* interactions and should be *real*. By introducing a real "pressure" field, $\Xi(\mathbf{r}) \equiv iW^*_+(\mathbf{r}) = -W_{+,I}(\mathbf{r})$, it is thus clear that eqs 58 and 61 can be discarded, leaving two equations, eqs 59 and 60, to determine the two real fields $\Xi(\mathbf{r})$ and $W(\mathbf{r}) \equiv W^*_{-,R}(\mathbf{r})$. These two equations are *exactly* those used in SCFT studies of AB diblock copolymers.[40]

Overall, we see that it is possible to use general knowledge of the location of saddle points in the complex plane to halve the computational effort required to compute them. There is *an important and subtle point*, however, associated with this reduction in size of the problem. The transformation $iW^*_+ \rightarrow \Xi$ with Ξ real implies that one is searching for saddle points along the imaginary W_+ axis in Figure 3. This is orthogonal to the physical (real) path of integration in the starting model. While H_R would have a *local minimum* at a saddle point along some permissible deformation of the physical path (e.g., the dashed path in Figure 3), H_R has a *local maximum* when the saddle point is approached along the Ξ direction. This feature is obviously very important to take into account when devising computational algorithms.

B. Spectral Methods. There are two general classes of techniques that have been applied to solving SCFT equations and hence to the numerical computation of inhomogeneous saddle points. The first are *spectral methods*, which attempt to represent the various spatially varying fields in a truncated Fourier-like basis. Alternatively, the nonlinear equations can be tackled in *real space* by suitable finite difference or finite element discretization of a computational domain. For the purpose of explaining the various methods, it is convenient to continue to work in the context of the incompressible AB diblock copolymer model.

A spectral method was first applied to the solution of the SCFT equations for AB diblock copolymers by Matsen and Schick in 1994.[40] Since that time, the method has been used to treat a large number of systems including block and graft copolymers of various architectures, copolymer blends, ABC triblock copolymers, three-component polymer emulsions, and polymer−polymer interfaces.[48,52−54] Other than the application to a wide variety of systems and extension to other

ensembles, the method has undergone little conceptual development in recent years. Nevertheless, it remains one of the most powerful and versatile techniques for the numerical computation of saddle points arising from field theory models of polymers and complex fluids.

The essence of the Matsen−Schick method is to expand the various spatially varying functions in the saddle point equations in a restricted Fourier basis. For example, in a SCFT study of incompressible diblock melts, eqs 59 and 60 are rewritten in terms of the fields Ξ and W, and these fields expanded according to

$$\Xi(\mathbf{r}) = \sum_{j=1}^{\infty} g_j f_j(\mathbf{r}),\ W(\mathbf{r}) = \sum_{j=1}^{\infty} w_j f_j(\mathbf{r}) \qquad (62)$$

The basis functions $f_j(\mathbf{r})$, $j = 1, ..., \infty$ are a complete orthogonal basis that are selected on two criteria: (i) the functions are eigenfunctions of the Laplacian operator ∇^2, and (ii) the functions have the same crystallographic symmetries as the complex fluid phase whose saddle point is being computed. Thus, for example, the basis functions corresponding to a lamellar phase of a block copolymer system (one-dimensional field variations) are the usual sines and cosines of trigonometric Fourier series. In contrast, the basis functions of the bicontinuous cubic "gyroid" phase (symmetry group $Ia\bar{3}d$) for AB diblocks are considerably more complicated, but are tabulated in standard crystallography texts.[55] In practice, the series in eq 62 are truncated after a finite number of terms, N_c, which leaves $2N_c$ expansion coefficients, (g_j and w_j for $j = 1, ..., N_c$) to be determined. The required $2N_c$ equations for these coefficients are obtained by projecting eqs 59 and 60 onto this truncated basis and invoking orthogonality.

The set of algebraic equations that arises from the above procedure is highly nonlinear because of the complicated functional relationships between the potential fields W,Ξ and the reduced density operators ϕ_A,ϕ_B. These relationships are summarized by eqs 30 and 46−48. Because of the choice of basis functions, terms such as $\nabla^2 q$ in the diffusion equations are *local* in the spectral representation, while the terms ψq and $\psi^\dagger q^\dagger$ are local in real space, but are highly *nonlocal* in the spectral representation. Nevertheless, the s-dependence can be explicitly integrated out of the diffusion equations once expressed in the Fourier basis. Overall, the computational effort involved in relating the expansion coefficients of the ϕ_K operators to the $\{g_j,\ w_j\}$ coefficients is comparable to the effort required to invert a matrix of rank $2N_c$ that is not narrow band diagonal, i.e., on the order of ${N_c}^3$ operations for large N_c.[50] This is the most expensive step in the calculation.

The details of converging the solution of the $2N_c$ nonlinear equations are not explicitly described in the papers of Matsen and Schick, but they apparently use a type of quasi-Newton algorithm similar to the Broyden method.[51] Shi and Noolandi[56] and Shull[57] describe an alternative Picard iteration procedure. In devising such methods it is important again to emphasize that the energy functional is to be *maximized* with respect to the g_j coefficients and *minimized* with respect to the w_j coefficients.

Overall, the Matsen−Schick spectral method is very powerful. By restriction of the search for saddle points in a restricted partition of function space with the crystallographic symmetries of a particular mesophase, the computational effort can be reduced (i.e., less basis functions need be employed) relative to other methods. Periodic boundary conditions with the appropriate symmetry are also naturally incorporated, so that computations of bulk system properties are devoid of finite-size effects. Moreover, in cases of weak to intermediate segregation ($\chi N < 50$) calculations of very high accuracy can be performed. This is particularly important in sorting out the mean-field phase diagrams of block copolymers, where small differences in H_R among the various saddle points are often encountered. As an example of such calculations, we reproduce in Figure 4 the SCFT phase diagram obtained by Matsen and Bates by applying the spectral method to the AB diblock copolymer model described here.[58] These and related calculations have proved extremely useful in guiding experiments on a variety of block and graft copolymer systems.

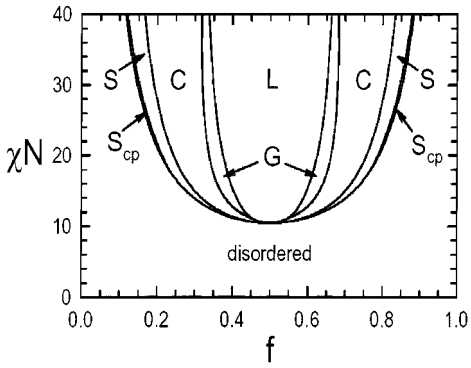

Figure 4. Mean-field phase diagram for the incompressible AB diblock copolymer model described in eqs 28−31, computed using the spectral method of Matsen and Schick. Regions denoted L, G, C, S, and S_{cp} correspond, respectively, to regions of stability of lamellar, gyroid, cylindrical, spherical (bcc), and spherical (close-packed) mesophases. Reprinted from ref 58. Copyright 1996 American Chemical Society.

The Matsen−Schick method has two principal limitations. The first is that it requires that the *symmetry* of a mesophase be specified in advance so that a proper set of basis functions can be utilized. In simple AB block and graft copolymer systems, there are normally a small number of competing structures (i.e., lamellae, cylinders, spheres, and gyroid), so one simply computes saddle points for all of them and uses the relative values of H_R to sort out relative thermodynamic stability. However, in the case of more complicated ABC type copolymers (or even ABCD copolymers!) the possibilities for self-assembly are enormous. Thus, it is necessary to use some physical intuition in limiting the selection of relevant saddle point structures to a reasonable number. Such a procedure, however, is bound to overlook some interesting and potentially useful forms of self-assembly. The second limitation of the Matsen−Schick method is encountered under stronger segregation conditions ($\chi N > 50$) or for complex three-dimensional structures, where many basis functions are required to obtain accurate numerical results. The computational effort evidently scales as ${N_c}^3 N_{iter}$, where N_{iter} is the number of iterations required to converge a solution to the set of $2N_c$ nonlinear algebraic equations. Evidently $N_{iter} = O(N_c)$ with the quasi-Newton convergence scheme, so the overall effort scales as N_c.[4] When N_c grows beyond about 500, supercomputer-like resources are required to implement the method.

The Matsen−Schick method has been extended to thin films[59] and to the study of topological defects in

copolymer mesophases,[60] where basis functions satisfying particular boundary conditions are required. While there has been very little work carried out with non-Fourier bases, Chebyshev polynomials, wavelets, or other strategies for representing the relevant fields, such approaches could prove to be useful in extending and/or improving spectral methods. Overall, we expect to see further developments in this proven methodology for implementing SCFT.

C. Real Space Methods. One of the earliest real space attempts to numerically compute inhomogeneous saddle points of field theory models of polymers was by Helfand and Wasserman in the context of AB diblock and ABA triblock copolymers.[61] These authors approximated the Wigner−Seitz cells of the lamellar, cylindrical, and spherical mesophases by rectangles, circles, and spheres, respectively, so that the SCFT equations could be reduced to one-dimensional form in Cartesian, polar, and spherical coordinates, respectively. The resulting equations were solved within a single Wigner−Seitz cell by a finite difference scheme. This strategy is computationally very advantageous, but it introduces unnecessary approximations and again requires the symmetry of the mesophase to be known in advance. Moreover, the Helfand−Wasserman approach would be difficult to apply to a complex, three-dimensional phase such as the gyroid structure. In more recent years, this general strategy has been extended and applied extensively by Whitmore, Noolandi, and co-workers,[62] Shull,[57] and Balazs.[63] Another popular variant of the Helfand−Wasserman method, which has been extensively applied in colloid and interfacial science, is the lattice formulation of Scheutjens and Fleer.[64]

A promising alternative real space strategy for implementing SCFT is the dynamic density functional theory (DDFT) method of Fraaije and co-workers.[65−67] Similar approaches have been adopted by Hasegawa and Doi,[68] Yeung and Shi,[69]and Reister et al.[70] Another closely related formalism is the lattice mean field theory of Coalson and Duncan,[42,71] which has primarily been applied to charged polymer systems. While DDFT is normally presented as a strategy for modeling structural evolution in inhomogeneous polymers, if run to equilibrium, the algorithm converges to saddle points of the field-theory models described here. *Thus, equilibrium structures computed with DDFT in fact represent solutions of the SCFT equations.* In simplest form, say applied to an AB diblock copolymer melt, the DDFT time evolution equations are written as diffusion equations for the average species-K monomer densities, $\rho_K(\mathbf{r}, t)$, (K = A or B):[66]

$$\frac{\partial \rho_K}{\partial t} = D_K \nabla \cdot [\rho_K(\mathbf{r}, t) \nabla \mu_K(\mathbf{r}, t)] \qquad (63)$$

where the D_K are species diffusion coefficients. The "intrinsic" chemical potentials $\mu_K(\mathbf{r}, t)$ are linearly related to (in our notation) Im$[\delta H/\delta W_+]$ and Re$[\delta H/\delta W_-]$ and amount to linear combinations of the monomer densities ρ_K and their conjugate (real) mean-field chemical potentials $W_K(\mathbf{r}, t)$. In our notation, $\Xi = W_A + W_B$ and $W = W_A - W_B$. When equilibrium is achieved in the DDFT method, the two intrinsic chemical potentials μ_K achieve **r**- and *t*-independent constant values. The *equilibrium* equations $\mu_K(\mathbf{r},\infty) = C_K$, where the C_K are constants, are exactly those of SCFT.

The DDFT algorithm proceeds by discretizing the various fields within a simulation box on a regular lattice. Finite difference approximations are applied. Fraaije and co-workers integrate eq 63 forward in time with a semi-implicit Crank−Nicholson scheme.[50] At each time step, the chemical potentials W_K entering μ_K must be deduced by inverting the functional relationship $\rho_K(\mathbf{r}, t;[W_A, W_B])$ that is manifest in eqs 46 and 47. Specifically, guesses are made for the W_K fields, the diffusion equations for q and $q^\dagger$ are solved numerically, and formulas like eqs 46 and 47 are used to construct the ρ_K. This procedure is iterated until W_K fields are obtained that produce the ρ_K fields at the current time step in the dynamical evolution. Fraaije and co-workers employ an explicit scheme for integrating the diffusion equations for the chain propagators.

The above implementation of DDFT has been fruitfully applied to a large number of polymeric systems, and a commercial version of the software is now available under the name of MesoDyn.[72] An important advantage of the DDFT method over the spectral method previously discussed is the fact that *no symmetry assumption about the mesophase being computed is required*—the partial differential equations are solved by simply imposing periodic boundary conditions on the overall simulation cell. As in a conventional particle-based computer simulation, one must be careful of finite-size effects, but provided that the cell dimension L exceeds the period of the mesophase structure by a factor of approximately 10, mesophases appear in the center of the cell quite independent of the shape or size of the system. (While finite-size effects are reduced upon increasing L, defects become more prevalent and more costly to anneal out of a simulation cell.) Thus, it is possible to use the DDFT technique to explore the phase diagrams of complicated types of polymer solutions, melts, or blends, e.g., ABC block copolymer alloys, where a rich variety of possibilities for self-assembly exist and where experimental results are lacking.

The primary disadvantage of the DDFT method is that it is a rather *inefficient* method to compute saddle points, i.e., *equilibrium solutions* of the SCFT equations. This is somewhat counterbalanced by its ability to provide some information about polymer dynamics, although its capability in this area is rather limited—viscoelastic and hydrodynamic effects and chain entanglements are not properly captured. There are two sources of inefficiency in the use of DDFT for computing equilibrium structures. The first is that the W_K fields, appearing in μ_K and required to determine future evolution of the structure, are determined by iteratively solving the diffusion equations for q, $q^\dagger$ until the current ρ_K fields are produced. This is the most computationally demanding step of the entire procedure. For a lattice with N_g sites, a numerical solution of the q, $q^\dagger$ diffusion equations requires of order (see below) $N_g N_s$ operations, where N_s is the number of s contour steps used to resolve the chain propagator over $0 < s < 1$. This procedure must be iterated N_w times to find the W_K's that reproduce target ρ_K fields, so the overall cost of this step in the algorithm is of order $N_g N_s N_w$. For a cubic box with 32 lattice sites on a side and assuming crude chain resolution, $N_s \approx 50$, and about 10 iterations to find the W_K's, $N_w \approx 10$, over 1×10^7 operations are required at each time step!

The second source of inefficiency in the DDFT method for computing equilibrium structures is that the diffusive dynamics employed in eq 63 inherently limits the rate of equilibration. While eq 63 is the simplest of the

various dynamical models employed in DDFT, it implies a local conservation of the species densities that acts to constrain and slow the dynamical evolution.

A final note is in order regarding the DDFT method. Practitioners often add a random (thermal) noise term to the right-hand side of evolution equations such as eq 63. This noise is usually taken to be Gaussian distributed with zero mean and with a second moment selected to satisfy a fluctuation−dissipation theorem. Naively, one might think that such a stochastic version of the method would extend its validity beyond the mean-field approximation. *This proves not to be the case.* As is clear from the previous sections, field theory models of soft materials are intrinsically complex with statistical weights that are not positive definite. Only saddle point field configurations can be computed with purely real methods; a complete theory requires special sampling methods that are the subject of the next section. Thus, a stochastic version of a purely real DDFT cannot generate equilibrium distribution functions that exactly capture the field fluctuations inherent in a model like eq 28. It follows that stochastic versions of DDFT are neither suitable for studying corrections to mean-field theory (i.e., beyond SCFT) nor suitable for analyzing fluctuation effects on phase transitions in complex fluids.

Our group has recently developed alternative real space strategies for computing saddle points that appear to be more efficient than the DDFT method.[73,74] Like DDFT, we devise a relaxational dynamics to find equilibrium solutions of the SCFT equations. Thus, our methods also do not require the symmetry assumption inherent in the spectral approach and can be used for "computational−combinatorial screening" of complex physical models with large parameter spaces to "prospect" for new phases and types of self-assembly. Unlike DDFT, we *do not attempt to construct dynamical trajectories that have physical significance*—we simply view the dynamical evolution as one of many possible nonlinear optimization strategies.

A clue for how to proceed was suggested by the work of Maurits and Fraaije.[67] They considered an alternative dynamical evolution strategy, referred to as "external potential dynamics" (EPD), in which the chemical potential fields, $W_K(\mathbf{r}, t)$, are viewed as the fundamental dynamical variables rather than the monomer densities. This approach has the advantage that the "intrinsic" chemical forces driving the dynamics of the W_K can be expressed in closed form in terms of $\rho_K(\mathbf{r};[W_A, W_B])$, which requires only *one* pass of solving the single-chain diffusion equations to evaluate at a current value of the W_K fields. The computational effort per time-step is thus reduced by a factor of N_w (from the DDFT method) to $N_g N_s$ operations. This would be expected to produce an order of magnitude reduction in run time. In presenting our numerical strategy, we depart from the EPD scheme as originally formulated in order to sacrifice realistic polymer dynamics for more rapid convergence to saddle points. This addresses the second source of inefficiency in the DDFT method described above.

Our approach is to write *nonconserved* relaxational dynamics for the relevant components of the chemical potential fields. For example, in the case of the AB diblock copolymer model, we use

$$\frac{\partial}{\partial t} W_{+,\mathrm{I}}(\mathbf{r}, t) = -\lambda_+ \mathrm{Im}\left[\frac{\delta H[W_+, W_-]}{\delta W_+(\mathbf{r}, t)}\right] \quad (64)$$

$$\frac{\partial}{\partial t} W_{-,\mathrm{R}}(\mathbf{r}, t) = -\lambda_- \mathrm{Re}\left[\frac{\delta H[W_+, W_-]}{\delta W_-(\mathbf{r}, t)}\right] \quad (65)$$

where $\lambda_\pm > 0$ are arbitrary relaxation rate coefficients. Clearly, if these dynamics converge to an equilibrium structure, the SCFT (saddle point) eqs 59 and 60 are satisfied. The next step is to replace $W_{+,\mathrm{I}}$, $W_{-,\mathrm{R}}$ with the real fields Ξ, W, noting that $\Xi = -W_{+,\mathrm{I}}$, which inverts the sign of eq 64 and ensures that H_R is to be maximized with respect to the "pressurelike" Ξ coordinates. After inserting the explicit expressions for the functional derivatives in the block copolymer model, this leads to

$$\frac{\partial}{\partial t} \Xi(\mathbf{r}, t) = \lambda_+[\phi_{A,R}(\mathbf{r}, t;[\Xi, W]) + \phi_{B,R}(\mathbf{r}, t;[\Xi, W]) - 1] \quad (66)$$

$$\frac{\partial}{\partial t} W(\mathbf{r}, t) = \lambda_-[\phi_{A,R}(\mathbf{r}, t;[\Xi, W]) - \phi_{B,R}(\mathbf{r}, t;[\Xi, W]) + 1 - 2f - 2(\chi N)^{-1} W(\mathbf{r}, t)] \quad (67)$$

It is straightforward to implement the above relaxation scheme. As in the DDFT method, a simulation cell is discretized using a uniform lattice. Overall periodic boundary conditions are applied. Continuous functions of $\mathbf{r}$ are sampled at the discrete lattice sites and finite difference approximations are used to compute spatial and temporal derivatives. For a lattice with N_g sites, the potential fields Ξ and W can thus be viewed as N_g-dimensional vectors; the overall configuration space is $2N_g$-dimensional. Simulations are started by initializing the Ξ and W vectors. This can be done with a random number generator if "random" initial conditions are desired. Such a starting point has the advantage of not biasing the saddle point search procedure toward any particular mesophase symmetry. Alternatively, an initial condition for the Ξ, W vectors with a particular inhomogeneous pattern can be used to "template" a rapid convergence to a saddle point with a desired symmetry.

Given an initial potential field configuration, the discretized diffusion equations for q, $q^\dagger$ are integrated forward in the contour variable s from the uniform initial condition to $s = 1$. We have found that an alternating direction implicit (ADI) scheme,[50] which is a higher dimensional extension of the Crank−Nicholson method, is particularly effective. Since the diffusion equations must be solved at every time-step (update of the Ξ, W fields), an efficient algorithm for their solution is critical. An advantage of the ADI method, which uses operator splitting, is that it reduces the necessary matrix algebra to inversion of tridiagonal matrixes, which can be performed in $O(N_g)$ operations. Overall, the work to solve the diffusion equations is of order $N_g N_s$ operations, as previously indicated.

Having solved the diffusion equations, the reduced density operators can be composed via eqs 46−47, so that the right-hand sides of eqs 66 and 67 are specified at the starting configuration. A simple explicit, first-order forward time scheme is then used to update the potential field vectors Ξ, W at the next time-step according to eqs 66 and 67. The relaxation rates $\lambda_\pm$ can be chosen independently and ideally as large as possible to accelerate convergence, but not so large as to cause

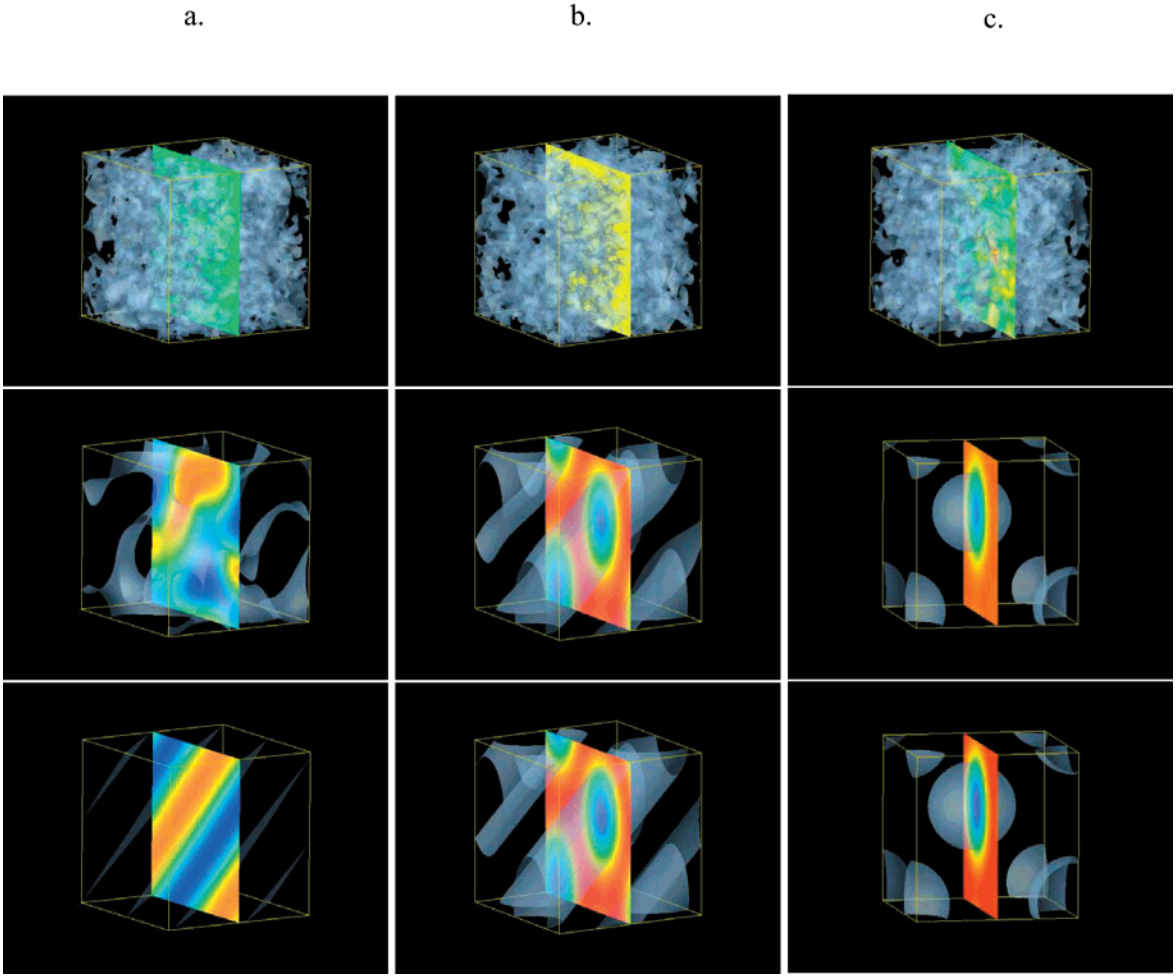

Figure 5. Time evolution (top to bottom), starting from random initial conditions, leading to converged three-dimensional lamellar, cylindrical, and spherical saddle points for an incompressible AB diblock copolymer melt. The top panels show isosurfaces of species A volume fraction $\phi_A(\mathbf{r}) = f$, which serve as the initial conditions in each case. The lower panels are isosurfaces defined by $\phi_A(\mathbf{r}) = 0.5$. The periodic simulation cell consisted of a lattice of 32^3 sites and $N_s = 100$, $\chi N = 16$. in all runs. Columns correspond to: (a) lamellae, $L = 6.4$, $f = 0.5$; (b) cylinders, $L = 5.76$, $f = 0.68$; and (c) spheres, $L = 4.8$, $f = 0.72$.

instability. Finally, this process of solving the diffusion equations for q, $q^\dagger$ and updating the potential fields is iterated until some convergence criterion is met (e.g., changes in H_R below some tolerance). The effort involved to find a saddle point is thus of order $N_g N_s N_{iter}$, where N_{iter} is the number of iterations (time-steps) required to obtain convergence. In practice, it appears that for the present relaxation scheme, N_{iter} is approximately independent of the lattice resolution N_g and the chain contour resolution N_s.

Given that saddle points can be located by such a method, how can one address the questions of section IV.A? In particular, can we find all relevant saddle points with the algorithm and can we be sure that we have located all the thermodynamically significant ones? The short answer, based on our experience with the algorithm and a variety of models,[73,74] seems to be that by starting from random initial conditions and by sufficient variations of those initial conditions, all thermodynamically relevant saddle points can be computed. We have seen a few instances where (at fixed parameter values) a particular random seed would lead to a metastable saddle point, while most random seeds would lead to a stable saddle point (lower value of H_R). Evidently, this indicates that the basin of attraction in configuration space is larger for the thermodynamically relevant saddle points. Nevertheless, with all such nonlinear optimization algorithms, one must be very careful about claiming to have found the optimal solution, i.e., a global as opposed to local minimum. Our *experimental* counterparts, however, have much the same problem—ABC block copolymers are notorious for their propensity to form metastable structures!

Some examples of saddle points (mean-field solutions) computed with the above algorithm are shown in Figures 5−7. Figure 5 shows panels of the time evolution (top to bottom), starting from random initial conditions, leading to converged three-dimensional lamellar (a), cylindrical (b), and spherical (c) phases for an incompressible AB diblock copolymer melt. The periodic simulation cell consisted of a lattice of 32^3 sites and with side length varying from $L = 4.8$ to $L = 6.4$. The computational effort per converged structure is about 10 h on a single 1.2 GHz CPU. Figure 6 shows saddle points obtained by computational exploration of a region of the five-dimensional parameter space ($\chi_{AB}N$, $\chi_{AC}N$, $\chi_{BC}N$, f_A, f_B) for a model of incompressible ABC miktoarm star−block copolymer melts[75] in two-dimensions. Finally, Figure 7 shows an isodensity surface [$\phi_C(\mathbf{r}) = 0.5$] for a saddle point computed for a model of an incompressible linear ABC triblock copolymer melt. The structure is tricontinuous, with "gyroidlike" struts of

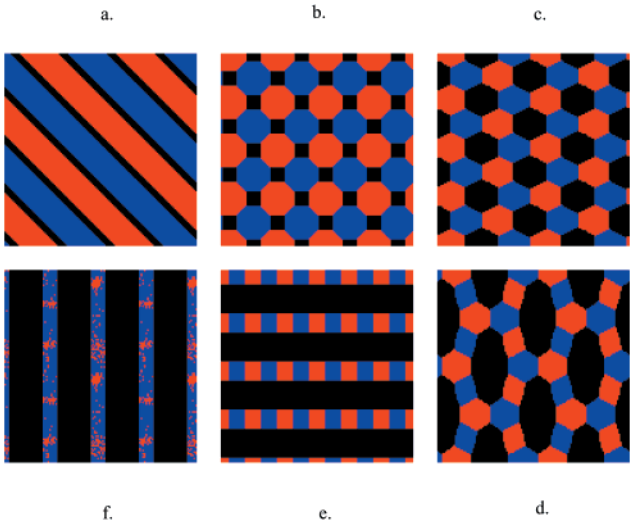

Figure 6. Saddle points obtained by computational exploration of the parameter space for a model of incompressible ABC miktoarm star−block copolymer melts in two-dimensions. Simulations were carried out on a 60 × 60 square lattice with $L = 6$, $\Delta s = 0.005$, $\chi_{AB} = \chi_{BC} = \chi_{AC}$, and $\chi_{AB}(N_A + N_B + N_C) = 30$. In panels a−f the relative size of the A arms (black) is systematically increased, while the B (red) and C (blue) arms are maintained at equal lengths, $f_B = f_C$. Clockwise: (a) $f_A = 0.20$, (b) $f_A = 0.22$, (c) $f_A = 0.38$, (d) $f_A = 0.46$, (e) $f_A = 0.54$, and (f) $f_A = 0.62$.

species C that are coated with a shell of species B. Similar core−shell gyroid structures have been reported in experiments by Shefelbine et al.[76] Evidently this real space strategy for computing saddle points is a powerful tool for mapping out the phase diagrams of complex polymer systems.

Overall, the advantages of our real space method are much the same as those of DDFT, although the strategy is considerably more efficient for the reasons described above. No symmetry assumption is required, other than overall periodic boundary conditions on the simulation cell, but one does have to be careful about finite-size effects. These are generally investigated by changing the box length L, while maintaining a fixed level of spatial resolution.

In facing a new problem, how does one decide between the real space and spectral approaches to implementing SCFT? As we have previously indicated, the computational effort required to carry out the spectral method is of order $N_c^3 N_{iter}$ operations, while the real space algorithm just discussed requires of order $N_g N_s N_{iter}$ operations. Obviously there are distinct prefactors in these scaling expressions and N_{iter} is different in the two cases. If the competing phases are *not known in advance*, we recommend an initial screening of the parameter space using the real space SCFT algorithm. To explain this, we note that if only overall periodic-cell symmetry is imposed, an *unrestricted* Fourier decomposition using N_c basis functions would be expected to give a comparable spatial resolution as a real space calculation with $N_g \approx N_c$ lattice sites. The $O(N_c N_s)$ scaling of the effort involved in the real space algorithm per convergence step would thus seem to favor that method over a spectral method [with an effort that is $O(N_c^3)$ per step] when "prospecting for new phases." If the symmetries of the phases are established in advance, however, a symmetry-restricted Fourier basis can be used to significantly reduce N_c required for convergence in the spectral method. In such cases (and for not too large χN), $N_c^3 \ll N_g N_s$, and the Matsen−Schick algorithm has a clear advantage over the real space approach for computing a saddle point of known symmetry.

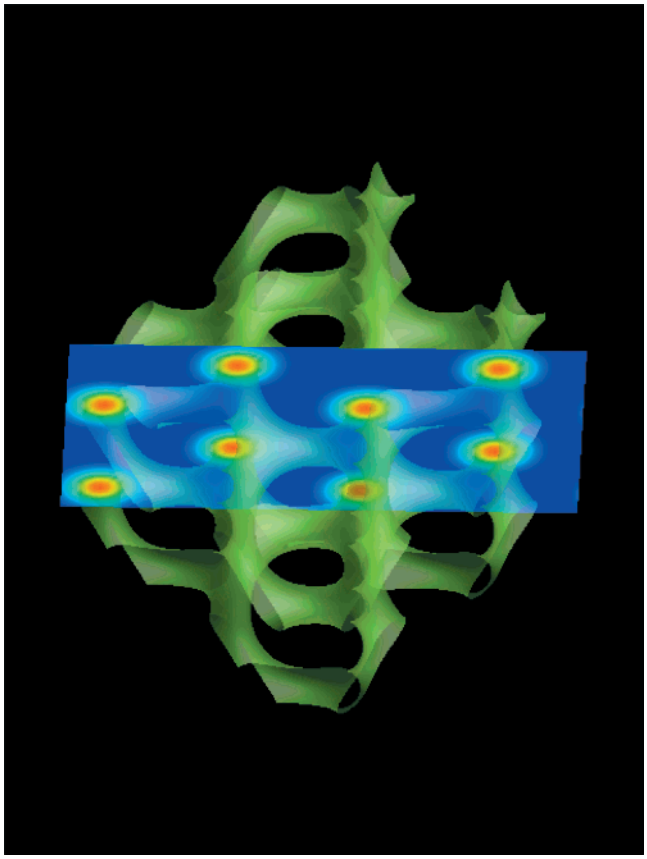

Figure 7. Isodensity surface, $\phi_C(\mathbf{r}) = 0.5$, of a computed saddle point for an incompressible model of a linear ABC triblock copolymer melt. The computed structure is tricontinuous with a "gyroidlike" network of species C that is coated with a concentric shell of species B. Calculations were done on a 40^3 lattice in a cubic box with the following parameters: $\Delta x = 0.16$, $\Delta s = 0.01$, $f_A = 0.41$, $f_B = 0.41$, $\chi_{AB}N = 28$, $\chi_{AC}N = 57$, and $\chi_{BC}N = 22$.

Obviously, many variations of the real space algorithm are possible. Finite element methods have recently been applied with uniform meshes;[77] future use of adaptive, unstructured meshes may permit the study of much larger, three-dimensional systems than are presently possible. Parallel computing strategies also appear very attractive.[78] The diffusion equations for q and $q^\dagger$ can be solved at the same time (without communication) for a particular realization of the potential fields. This "natural" parallelism is particularly important to exploit when more than two chemical species are involved and thus larger numbers of diffusion equations are to be solved. Spatial decomposition to promote parallelism is also possible and highly desirable if a dedicated cluster is available. Another potential route to faster algorithms is to use analytical methods to approximate, rather than exactly compute, the single chain partition function Q. This avoids the expense of constructing numerical solutions to diffusion equations such as eq 16. Bohbot-Raviv and Wang[79] have recently adopted such a strategy; undoubtedly much room exists for developing improved approximations for the nonlocal functionals, e.g., $Q[iW]$, that enter the field theories. Finally, we note that the relaxation scheme outlined in eqs 64 and 65 is the simplest possible among nonlinear

optimization strategies. Undoubtedly, more sophisticated schemes could be devised that would accelerate convergence.

V. Beyond Mean-Field Theory: Sampling Methods

In the previous section we discussed strategies for finding stationary field configurations of the effective Hamiltonian H for field theory models of polymers and other complex fluids. These stationary configurations (saddle points) are significant in that they represent a mean-field approximation to the thermodynamic properties of a particular phase of the system. Moreover, each inhomogeneous phase with a distinct symmetry can be associated with a saddle point possessing that same symmetry. In application to polymers, we are fortunate in that mean-field theory (i.e., SCFT) proves to be surprisingly accurate when used to describe dense systems of high molecular weight polymers, such as concentrated polymer solutions, molten blends, block copolymers, and their alloys. This fortunate situation highlights the power of field-theoretic models: by simply computing stationary points, we can obtain useful and accurate approximations to the thermodynamic properties of a dense, multicomponent polymer system. In contrast, energy minimization of a particle-based model for a dense polymer system proves far less valuable.

We can understand the accuracy of mean-field theory for concentrated polymer phases by recalling the discussion of section III.B. In both the polymer solution model and the diblock copolymer model, we saw that a dimensionless chain concentration, $C \equiv nR_{g0}^d/V$, controls the amplitude of field fluctuations about saddle points and thus the accuracy of SCFT. Such a parameter is often referred to as a "Ginzburg parameter."[30] In a polymer melt, the concentration of chains, n/V, is inversely proportional to the degree of polymerization N, so $C \sim N^{d/2 - 1}$ or $C \sim N^{1/2}$ in three dimensions. It follows that $C \to \infty$ for $N \to \infty$, so SCFT becomes exact in the limit of infinite molecular weight. Obviously, in tackling a new polymer system with field-theoretic methods, the computation of saddle points (implementing SCFT) is a very good place to start.

Nevertheless, there are quite a number of physical situations where mean-field theory is known to be inaccurate. Dilute and semidilute polymer solutions are a prime example.[15,35] Polymer blends near a critical point, block copolymers near the order−disorder transition (ODT),[80] and polymeric microemulsions[81−83] are other notable cases where SCFT fails. In such instances, we require a method for numerically sampling the field fluctuations in a complete model, i.e., a field-theoretic simulation (FTS) method, to accurately compute structure and thermodynamic properties.

A first step toward implementing a FTS method for the case of microphase separated block copolymers was introduced by Shi, Noolandi, and co-workers.[56,84] These authors formally carried out the steepest-descent asymptotic expansion of the block copolymer model (described in section III.B) to one term beyond the leading saddle point approximation. This first correction term (the so-called "one-loop" fluctuation correction) is numerically rather involved to evaluate, in part because it depends on having previously computed the relevant inhomogeneous saddle point. A separate local analysis must be done around each saddle point to gain an understanding of the first effect of fluctuations on the global phase diagram.

The Shi−Noolandi approach has been fruitfully applied to examine the stability of ordered phases of diblock copolymers, to aid the interpretation of SAXS and SANS experiments on such systems, and to help identify kinetic pathways connecting the various ordered mesophases.[56,84] A fundamental limitation of the method is that it captures only the leading correction term in the steepest-descent expansion, so is expected to be accurate only for very large values of C. Indeed, in the case of the order−disorder transition (ODT) for a symmetric ($f = {}^1/_2$) diblock copolymer melt, we know that the behavior of the model for $1/C \to 0$ is a singular perturbation problem and that the steepest-descent expansion must be resummed to infinite order[80,85] to capture the leading fluctuation-induced shift in the transition temperature ($\sim C^{-2/3}$). Thus, the Shi−Noolandi formalism can only be safely applied in situations where field fluctuations remain small in amplitude. Finally, we note that a similar approach to computing one-loop fluctuation corrections has been described by Coalson and Duncan[42] in the context of a lattice field theory for electrolyte and polyelectrolyte solutions.

Over the past year, our group has been developing methods for direct numerical sampling of field theory models of soft materials in the absence of any approximations.[24] Ideally, such methods should be no more involved to implement than conventional particle-based computer simulation techniques. Fortunately, we can benefit from the extensive and rich literature on closely related lattice gauge theories that have been applied widely in nuclear, high energy, and hard condensed matter physics.[23,86]

To date, we have identified two general FTS strategies that appear to be promising for studies of soft materials, such as polymers and other complex fluids. The first is a *complex Langevin (CL) method* and the second is a class of *steepest-descent (SD) techniques*. We begin by discussing the SD method.

A. Steepest-Descent Sampling. It is convenient to introduce the SD method in the context of the polymer solution model, summarized by eqs 13−16. As was discussed in section II.A, it is possible to rewrite the partition function for such a model in the form

$$Z = \int \mathscr{D}[W] \cos(H_I[W]) \exp(-H_R[W]) \qquad (68)$$

where all quantities in the integrand are real and the path of integration is along the real W axis. A simple numerical strategy for sampling such an integral would be to discretize the spatial domain on a uniform lattice so that the real field $W(\mathbf{r})$ becomes a real N_g-dimensional vector $W^{N_g} \equiv \{W_j,\ j = 1,\ ...,\ N_g\}$ and the functional integral is replaced by a N_g-dimensional Riemann integral $\int dW^{N_g} \equiv \Pi_{j=1}^{N_g} \int dW_j$. A conventional Monte Carlo method could be used to generate a series of states in the configuration space with a probability distribution function proportional to the positive definite weighting factor $P(W^{N_g}) = \exp[-H_R(W^{N_g})]$. Averages of observables $G(W^{N_g})$ would then be computed by including an explicit factor of the phase factor, $\cos(H_I)$:[31,87]

$$\langle G(W^{N_g})\rangle = \frac{\langle G(W^{N_g})\cos[H_I(W^{N_g})]\rangle_P}{\langle \cos[H_I(W^{N_g})]\rangle_P} \qquad (69)$$

The average on the left-hand side of this equation

represents an ensemble average with the full (complex) statistical weight $\sim\exp[-H(W^{N_g})]$; the averages denoted by $\langle ...\rangle_P$ on the right-hand side are "time averages" over the Markov chain of configurational states sampled from $P(W^{N_g})$ in a Monte Carlo simulation.

The above approach has the advantage of simplicity; however, in practice it is not very useful. The integration path, which in this case is the real axis for each W_j, is *not* a constant phase or steepest descent (ascent) path, so the phase factor $\cos[H_I(W^{N_g})]$ oscillates in sign from state to state along a Monte Carlo trajectory. As a result, it proves very difficult to accurately compute the right-hand side of expressions such as eq 69.

One method of eliminating the strong oscillations in the integrand is to adopt a steepest-descent (SD) strategy, familiar in the asymptotic analysis of low dimensional integrals.[47] The approach is very similar to that used in section III.B to argue that the saddle point dominates the behavior of the model for $C \to \infty$. Specifically, we deform the path of integration as in Figure 2 onto a new path that passes through the relevant saddle point and is also a constant phase path to quadratic order near the saddle point. Indeed, for the simple homogeneous saddle point of the polymer solution model, we have already shown that this can be accomplished with the simple constant shift in field to $\tilde{W}(\mathbf{r}) = W(\mathbf{r}) + iBC$, which leads to eqs 52 and 53. Here we depart from the analysis of section III.B. Instead of using the representation of the model on the deformed path as a starting point for a large C expansion, we develop a computer simulation strategy around the new model summarized by eqs 52 and 53. It is important to note that there is *no approximation invoked*—these equations represent an exact reformulation of the polymer solution model.

Our simulation strategy is to adapt the sampling method described above with a few modifications. The field $\tilde{W}(\mathbf{r})$ is replaced by a real N_g-vector $\tilde{W}^{N_g}$. Required is an efficient algorithm that can generate a series of states in the configuration space $\tilde{W}^{N_g}$ with a probability distribution function proportional to the positive definite weighting factor $\tilde{P}(\tilde{W}^{N_g}) = \exp[-\tilde{H}_R(\tilde{W}^{N_g})]$. A simple Monte Carlo procedure with attempts to change the chemical potential $\tilde{W}_j$ of *single sites j* proves not to be the best choice. Each evaluation of the energy function $\tilde{H}_R$, which is required to make an accept/reject decision on the trial change, is expensive because of the *nonlocal* character of the effective Hamiltonian and requires of order $N_g N_s$ operations. Thus, a more efficient scheme is one that invokes *multiple-site trial moves* between energy evaluations. Our preference is a method known in the literature as "smart" or "hybrid" Monte Carlo simulation.[23,86,88,89] In such a method, at each MC step, one updates the value of the chemical potential(s) at all N_g lattice sites to construct a new trial configuration $(\tilde{W}^{N_g})'$. These individual site updates are carried out by summing (for the jth site) a systematic displacement term proportional to the "force" $-\partial\tilde{H}_R/\partial\tilde{W}_j$ with a random displacement. This is similar to a move in a Brownian dynamics simulation. After updating all N_g sites in this fashion (with the force computed only once!), an overall move of $\tilde{W}^{N_g} \to (\tilde{W}^{N_g})'$ is generated. This move is then accepted or rejected based on an acceptance probability criterion that enforces detailed balance and that differs in form from the usual Metropolis criterion because of the force-directed nature of the trial move. The net effect of many such MC sweeps is a Markov chain of $\tilde{W}^{N_g}$ states that are sampled from a probability distribution function proportional to $\tilde{P}(\tilde{W}^{N_g}) = \exp[-\tilde{H}_R(\tilde{W}^{N_g})]$. These states can be used to construct "time" averages for observables $G(\tilde{W}^{N_g})$ just as in eq 69:

$$\langle G(\tilde{W}^{N_g})\rangle = \frac{\langle G(\tilde{W}^{N_g})\cos[\tilde{H}_I(\tilde{W}^{N_g})]\rangle_{\tilde{P}}}{\langle \cos[\tilde{H}_I(\tilde{W}^{N_g})]\rangle_{\tilde{P}}} \qquad (70)$$

An important difference from the "naive" method of eq 69, however, is that now the sampling is carried out along a deformed path that is locally a constant phase path near the saddle point (at the origin in this case). Thus the sign oscillations in the weighting factor $\cos[\tilde{H}_I(\tilde{W}^{N_g})]$ are significantly reduced (but not completely eliminated because $\tilde{H}$ is generally not a simple quadratic form in $\tilde{W}^{N_g}$) and the convergence of the MC procedure is accelerated.

We have successfully applied the above SD sampling method to several problems, including two- and three-dimensional homopolymer solutions[90] and inhomogeneous solutions of strong electrolytes.[91] In these applications, there is a single analytically accessible saddle point about which to focus the SD analysis. In other situations, where the relevant models possess a number of competing saddle points, we have found that the SD method is either tedious to implement or the identification of an appropriate constant phase path is difficult or expensive to compute. For example, the incompressible diblock copolymer model of eqs 28 and 29 has multiple saddle points, as discussed in section III.B. Depending on the values of the relevant parameters, (χN, f, C), either the homogeneous, disordered phase saddle point at the origin, $W_\pm^* = 0$, or one of the inhomogeneous ordered phase saddle points can dominate the thermodynamic behavior. A *separate* SD analysis must be manually executed about each saddle point to map out the overall behavior of the model. Besides the obvious labor involved in such analysis, the constant phase paths through the *inhomogeneous* saddle points are not as straightforward to identify as in the simple polymer solution model and must be obtained numerically. Overall, a fundamentally different type of sampling method is clearly needed to conveniently simulate field theory models with many inhomogeneous saddle points.

B. Complex Langevin Sampling. The complex Langevin (CL) sampling method at least partially addresses this need. The CL method was originally developed by Klauder[92] and Parisi[26] as a strategy for sampling quantum field theories on a lattice and for simulating more general types of lattice gauge theories with complex actions. Such theories have the same characteristic nonpositive definite statistical weights as encountered in the field theory models described here.

To introduce the CL technique, we again return to the simple polymer solution model of eqs 13−16. It is important to emphasize that in applying the CL method, *saddle points and SD paths do not need to be determined in advance*; thus, the transformation of the model leading to eqs 52 and 53 is unnecessary. The basic idea behind the CL method is to stochastically sample the relevant field, i.e., $W(\mathbf{r})$, not just along the real axis, but in the *entire complex plane* of $W = W_R + iW_I$. Recall that

for some observable $G[W]$, the expectation (average) value can be expressed as

$$\langle G[W]\rangle = Z^{-1}\int \mathcal{D}[W_R]\exp(-H[W_R])G[W_R] \quad (71)$$

where we have explicitly noted that the path of integration is along the real axis, yet the statistical weight $Z^{-1}\exp(-H)$ is complex. In the CL method, the strategy is to instead express such an observable as

$$\langle G[W]\rangle = \int \mathcal{D}[W_R]\int \mathcal{D}[W_I]\, P[W_R, W_I]G[W_R + iW_I] \quad (72)$$

where the *complex* weight $Z^{-1}\exp(-H)$ has been replaced by a *real, positive definite* statistical weight $P[W_R, W_I]$, in return for extending the field to the complex plane. This extension has a practical cost in that the number of configurational degrees of freedom in a simulation is doubled, but in our experience this is an acceptable trade-off.

The statistical weight $P[W_R, W_I]$ is the steady-state limit (if it exists) of a more general (real) probability distribution functional $P[W_R, W_I, t]$ that gives the probability of observing the field configuration $W = W_R + iW_I$ at time t. This distribution can be generated by a stochastic "complex Langevin" dynamics defined by

$$\frac{\partial}{\partial t}W_R(\mathbf{r}, t) = -\mathrm{Re}\left[\frac{\delta H[W]}{\delta W(\mathbf{r}, t)}\right] + \eta(\mathbf{r}, t)$$
$$= -W_R(\mathbf{r}, t)/B + C\rho_I(\mathbf{r}, t;[W])/\rho_0 + \eta(\mathbf{r}, t) \quad (73)$$

$$\frac{\partial}{\partial t}W_I(\mathbf{r}, t) = -\mathrm{Im}\left[\frac{\delta H[W]}{\delta W(\mathbf{r}, t)}\right]$$
$$= -W_I(\mathbf{r}, t)/B - C\rho_R(\mathbf{r},t;[W])/\rho_0 \quad (74)$$

The field $\eta(\mathbf{r}, t)$ is a *real, Gaussian, white thermal noise source* with first and second moments given by

$$\langle\eta(\mathbf{r}, t)\rangle = 0, \langle\eta(\mathbf{r}, t)\eta(\mathbf{r}', t')\rangle = 2\delta(\mathbf{r} - \mathbf{r}')\delta(t - t') \quad (75)$$

An important feature of the CL equations is that the noise source appears *only* in the relaxational dynamics of the real part of the field. Note also that when the noise term is removed, the equations *relax to saddle points* of the theory and, indeed, eqs 73 and 74 reduce to the real-space saddle point algorithm described in eqs 64 and 65. Along a CL trajectory, the imaginary part of the field deterministically attempts to relax W_I to its saddle point value (cf. eq 51) at the instantaneous value of W_R. This has the net effect of a sampling path in the complex plane that automatically adjusts to approach a steepest path, which in the present case is a trajectory near the saddle point with $W_I = -BC$ constant. This automatic adjustment feature improves the convergence of the method (by minimizing phase oscillations) but also is particularly convenient because in a model with many competing saddle points, no particular saddle point need be isolated or analyzed.

The above coupled Langevin equations that define the CL method can be converted to the following Fokker–Planck equation for the probability distribution functional $P[W_R, W_I, t]$:

$$\frac{\partial}{\partial t}P[W_R, W_I, t] = \int \mathrm{d}\mathbf{r}\int \mathrm{d}\mathbf{r}'\,\frac{\delta^2 P}{\delta W_R(\mathbf{r}, t)\delta W_R(\mathbf{r}', t)} +$$
$$\int \mathrm{d}\mathbf{r}\,\frac{\delta}{\delta W_R(\mathbf{r}, t)}\{U_R(\mathbf{r}, t;[W])P\} +$$
$$\int \mathrm{d}\mathbf{r}\,\frac{\delta}{\delta W_I(\mathbf{r}, t)}\{U_I(\mathbf{r}, t;[W])P\} \quad (76)$$

where $U_R(\mathbf{r}, t;[W])$ and $U_I(\mathbf{r}, t;[W])$ represent the real and imaginary parts, respectively, of the complex derivative $\delta H/\delta W(\mathbf{r}, t)$. A general proof that eq 76 relaxes in time to a stationary distribution $P[W_R, W_I]$ that can be used to compute averages as in eq 72 is not available. Nevertheless, if a stationary distribution is achieved, which can be established in a simulation by expectation values becoming time independent, then it can be proved that the ensemble averages computed by using this distribution (i.e., with eq 72) are equivalent to ensemble averages computed with the original model (i.e., with eq 71).[27,28] In practice, we have encountered no problems with convergence or uniqueness of solutions in CL simulations. Nevertheless, it is important to check that averages converge to time independent values and that these values are independent of the initial conditions that were used to start the simulations.

To implement a CL simulation, a simulation cell is constructed from a uniform lattice with N_g sites. The complex field $W(\mathbf{r})$ is thus replaced by a $2N_g$-dimensional vector $W^{2N_g} \equiv (W_R{}^{N_g}, W_I{}^{N_g})$. Equations 73 and 74 are discretized in both space and time and iterated forward from an initial configuration to generate a Markov chain of configurational states. We generally start simulations from a random initial configuration or a saddle point, and use a simple first-order forward time, explicit scheme for the time integration. In the case of polymer models, i.e., in performing a FTPS simulation, the complex monomer density operator $\rho(\mathbf{r}, t;[W])$ must be evaluated at *each time step* by solving a complex diffusion equation such as eq 16 and by use of formulas such as eq 37. This is expensive, requiring of order N_gN_s operations, so it is imperative that the algorithms used to solve the diffusion equation are as efficient as possible.

After an equilibration period, the Markov chain of complex field configurational states can be used to approximate the ensemble average in eq 72 by a "time average" over the states of the chain. Specifically,

$$\langle G[W]\rangle \approx \frac{1}{M}\sum_{j=1}^{M} G[W_R{}^{N_g}(j) + iW_I{}^{N_g}(j)] \quad (77)$$

where the jth configurational state is denoted by $W_{R/I}{}^{N_g}(j)$. Assuming convergence, equality of ensemble and time averages is achieved for $M \to \infty$.

The size of the time step, Δt, in a CL simulation is dictated by considerations of stability, accuracy, and computational resources. Too large a time step can lead to instabilities and errors in computed averages [errors are $O(\Delta t^2)$ in the scheme described]; too small a time step leads to unnecessarily long runs. The lattice spacing Δx and simulation box size L are chosen to affect a compromise between accuracy and computational effort. We have found it convenient to fix Δx and L based on this compromise for one or more saddle point configurations in advance of starting a CL simulation. For example, a choice of these parameters that resolves

$|H|$ to three or four significant figures at the saddle point configuration of a lamellar block copolymer phase would be a good starting point for CL simulations to study fluctuations of that lamellar phase.

As an example of an application of the CL sampling method to carry out a FTPS simulation, we consider the model of an incompressible AB diblock copolymer melt introduced in section II.C. In this model, there are two independent chemical potential fields, $W_{\pm}(\mathbf{r})$, which must each be extended to the complex plane. Thus, the CL equations are a set of four coupled Langevin equations for the real fields $W_{+,\mathrm{R}}$, $W_{+,\mathrm{I}}$, $W_{-,\mathrm{R}}$, and $W_{-,\mathrm{I}}$. The first two equations, for example, are

$$\frac{\partial}{\partial t} W_{+,\mathrm{R}}(\mathbf{r}, t) = -\mathrm{Re}\left[\frac{\delta H[W_+, W_-]}{\delta W_+(\mathbf{r}, t)}\right] + \eta(\mathbf{r}, t) = C[\phi_{\mathrm{A,I}}(\mathbf{r}, t;[W_+, W_-]) + \phi_{\mathrm{B,I}}(\mathbf{r}, t;[W_+, W_-])] + \eta(\mathbf{r}, t) \quad (78)$$

$$\frac{\partial}{\partial t} W_{+,\mathrm{I}}(\mathbf{r}, t) = -\mathrm{Im}\left[\frac{\delta H[W_+, W_-]}{\delta W_+(\mathbf{r}, t)}\right] = -C[\phi_{\mathrm{A,R}}(\mathbf{r}, t;[W_+, W_-]) + \phi_{\mathrm{B,R}}(\mathbf{r}, t;[W_+, W_-]) - 1] \quad (79)$$

We have implemented a CL simulation of this model in two dimensions on a 64×64 square lattice with $L = 8$($V = L^2 = 64$, $\Delta x = 0.125$) and periodic boundary conditions. The diffusion equations for the (complex) q and $q^\dagger$ are solved with an ADI scheme and a contour step of $\Delta s = 0.025$. With these choices, $|H|$ is computed to three significant figure accuracy at the relevant lamellar and hexagonal saddle points of the model. Figure 8a shows the real part of the monomer A volume fraction field $\phi_{\mathrm{A,R}}$ at a computed hexagonal saddle point for parameters $\chi N = 15.2$ and $f = 0.3$. Figure 8b shows the instantaneous A species volume fraction after running a CL simulation for 120 000 time steps ($\Delta t = 0.1$) and for a small value of the Ginzburg parameter $C = 5$. Evidently, thermal fluctuations have "melted" the hexagonal phase in this case. At a larger value of $C = 100$, we see in Figure 8c (another snapshot after 120 000 CL time steps) that the hexagonal mesophase is again present but is distorted slightly by fluctuations in comparison with the saddle point configuration of Figure 8a. As expected, the fluctuations increase in intensity as C is reduced.

FTPS simulations similar to the above have been used to explore quantitatively the effect of fluctuations on shifting the order−disorder transition (ODT) in two-dimensional, symmetric ($f = 0.5$) diblock copolymer melts.[24] Figure 9 shows the shift in the ODT from the mean-field (SCFT) value of $(\chi N)_t$ ($C = \infty$) = 10.495 as a function of the Ginzburg parameter C. The ODT was identified in the simulations at each value of C by the visual observation of melting of the lamellar phase upon increasing χN. A best fit line through the data for $C \geq 128$ yields a slope of −0.68 for the asymptotic, large C shift in the ODT. This is remarkably close to the analytical prediction of $\Delta(\chi N) \sim C^{-2/3}$ obtained from a self-consistent Hartree analysis of fluctuation effects in diblock copolymers.[80,85] It is important to emphasize that such results would be very difficult to obtain by means of a conventional particle-based simulation of a highly incompressible block copolymer melt.

A few comments should be made about such lattice simulations that go beyond mean-field theory. First, the underlying lattice structure clearly breaks the continuous translational and rotational symmetries under which the energy functional is invariant (Goldstone modes). Thus fluctuations involving such modes will not be properly treated unless special care is taken to minimize pinning and other deleterious effects of the computational lattice. Another role the lattice plays is to provide a short-range ("ultraviolet") cutoff which regularizes the field theory. This cutoff, which can have sizable but generally uninteresting effects on the locations of phase boundaries and various thermodynamic

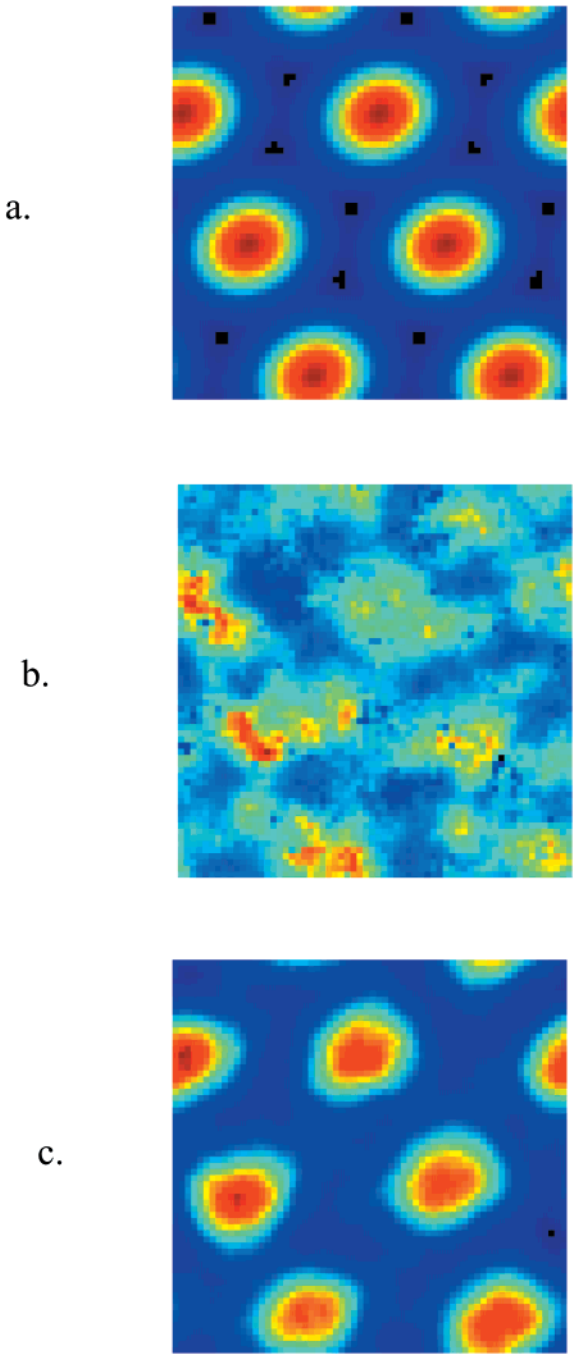

Figure 8. (a) Saddle point configuration of the species A monomer volume fraction field for a two-dimensional incompressible AB diblock copolymer melt with $\chi N = 15.2$ and $f = 0.3$. (b) Instantaneous configuration of the species A volume fraction field after 120 000 time steps of a complex Langevin simulation with $C = 5$. (c) Instantaneous configuration of the species A volume fraction field after 120 000 time steps of a complex Langevin simulation with $C = 100$.

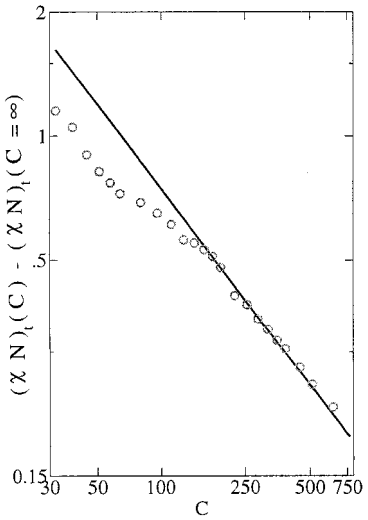

Figure 9. Fluctuation-induced shift in the order−disorder transition temperature (relative to the mean-field value of $\chi N = 10.495$) as a function of the Ginzburg parameter C for a two-dimensional, incompressible diblock copolymer melt. The best fit line for $C \geq 128$ yields a slope of -0.68.

quantities, is generally dealt with differently in analytical calculations of fluctuation phenomena. Thus, it is important to isolate such cutoff-dependent effects when comparing FTS data with analytical theories or experiment. In the above CL simulations of diblock copolymers, the magnitude of the fluctuation-induced shift of the ODT is sensitive to the lattice cutoff, but not the dependence of the shift on C.

As a second example of FTPS simulations with CL sampling, we have recently started to study a model of a ternary melt blend of A homopolymer, B homopolymer, and symmetric AB diblock copolymer. The primary focus is on blends of equal molecular weight A and B homopolymers (degree of polymerization N_H) mixed in equal proportions with varying amounts of symmetric ($f = {}^1/_2$) AB diblock copolymers (degree of polymerization N). In this restricted composition space (the so-called isopleth plane), and assuming overall melt incompressibility, the intensive thermodynamic properties are functions of four parameters: χN, C (defined here as the total number density of polymers made dimensionless by the unperturbed radius of gyration of a diblock copolymer), the molecular weight ratio $\alpha \equiv N_H/N$, and the average total (A + B) volume fraction of homopolymer ϕ_H.

This ternary blend model has been studied to date only in the mean-field (SCFT) approximation, which again corresponds to the $C \rightarrow \infty$ limit of the field theory.[81,93,94] The model is particularly interesting in that application of SCFT indicates the existence of an *isotropic Lifshitz point* in the isopleth plane, $(\chi N, \phi_H)$, for $\alpha < 1$. A Lifshitz point is a multicritical point delimiting mesophase separation behavior (in this case lamellar ordering) from macrophase separation behavior (in this case demixing into two phases, each rich in one of the two homopolymers). For the particular case of $\alpha = 0.5$, SCFT locates the Lifshitz point at $(\chi N)_L = 6$ and $(\phi_H)_L = 2/3$. A lamellar phase is predicted by mean-field theory to be formed when cooling such a blend with $\phi_H < {}^2/_3$ from the high-temperature disordered phase; a two-phase coexistence of homogeneous liquid phases is expected upon cooling blends with $\phi_H > {}^2/_3$. Indeed, Figure 10a shows the saddle point configuration of the

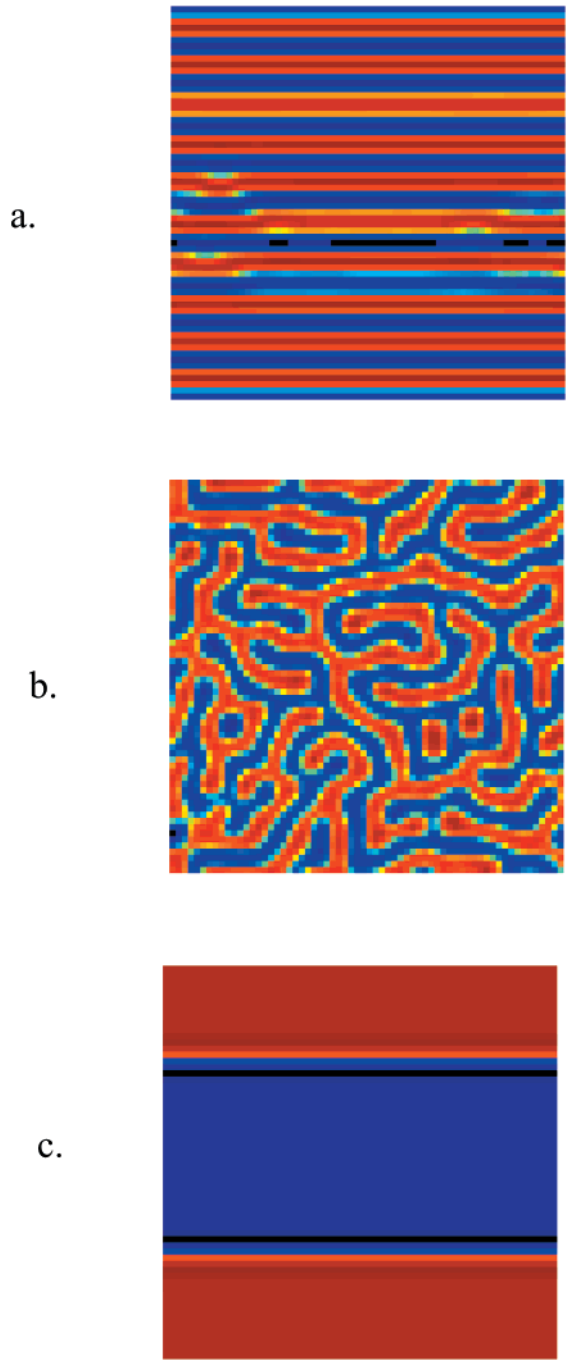

Figure 10. Real part of the total A monomer volume fraction field for a symmetric, ternary blend of A homopolymer, B homopolymer, and symmetric AB diblock copolymer. The homopolymers are mixed in equal proportions and have equal degrees of polymerization, $N/2$, half of the diblock copolymer degree of polymerization N. Relevant parameters are $\chi N = 9.5$, $L = 48$, and $\Delta x = 0.75$. Panels a and c denote saddle point configurations with total homopolymer volume fractions of $\phi_H = 0.45$ and $\phi_H = 0.8$, respectively. Panel b shows an instantaneous configuration after a 200 000 time step FTPS simulation (with CL sampling and $C = 100$) of a blend with an intermediate composition, $\phi_H = 0.65$, very close to the Lifshitz composition, $(\phi_H)_L = {}^2/_3$.

total A monomer volume fraction field arising from a two-dimensional real space calculation on a 64×64 lattice with $L = 48$, $\chi N = 9.5$, and $\phi_H = 0.45$. The configuration is clearly lamellar. Figure 10c shows the corresponding saddle point configuration for the same parameters, except that ϕ_H was increased to 0.8. This

configuration reflects a macroscopic phase separation in the simulation box (the two interfaces are forced by the periodic boundary conditions).

Experimental observations on such blends near a Lifshitz point suggest that thermal fluctuation effects are extremely strong and may even destroy the Lifshitz point, replacing it with a region of *bicontinuous polymeric microemulsion*.[82,83] Thus, the above blend model in the vicinity of the mean-field Lifshitz point is an excellent candidate for study by FTPS methods. Early results are very promising: Figure 10b shows a snapshot of the A monomer volume fraction field after 200 000 time steps of a two-dimensional FTPS simulation with CL sampling ($C = 100$), carried out very near the Lifshitz composition ($\phi_H = 0.65$). Thermal fluctuations have clearly created a highly structured, disordered microemulsion-like morphology. We plan to report more extensive results from FTPS simulations of this ternary blend model soon.[95]

VI. Discussion and Conclusions

In the present review, we have described a suite of field-theoretic computer simulation (FTS) tools for analyzing the equilibrium structure and thermodynamics of both simple and complex fluids. These methods are very versatile in that they allow models to be formulated at atomistic, mesoscopic, or macroscopic scales. Moreover, we have seen how field theory models suitable for study by FTS techniques can be derived from conventional particle-based models of fluids. Thus, it is possible to connect the potential parameters used in traditional MD or MC simulations to the parameters in field theory models amenable to study by the methods described here. Another attractive feature of building a computer simulation strategy around field theory models is that these are the same models commonly used in analytical studies aimed at extracting "universal" features of the structure and thermodynamics of polymers and complex fluids.[15] The FTS methods thus enable numerical studies of field theory models in parameter ranges or situations where approximate analytical tools are inadequate or fail. Finally, *experimental studies* of complex fluids are often interpreted in the context of parameters (e.g., Flory χ parameters) and predictions derived from field theory models. As a result, it is often more straightforward to connect experimental data to results from a FTS simulation than to numerical data from particle-based MD or MC simulations.

It is still too early in the development of FTS methods to make definitive statements about the conditions under which a FTS simulation strategy is favored over a conventional simulation approach. Nevertheless, our experience to date suggests the following:

•*Atomic and small-molecule fluids* are generally best studied by particle-based simulation methods. For typical interparticle potentials with harsh repulsions at small separations, a rich liquid structure is set up on atomic scales that is manifest, e.g., in the radial distribution function. While such atomic-scale liquid structure can be captured in FTS simulations, it requires a very high lattice resolution. Thus, one expects that more degrees of freedom would be required for a FTS study of a small molecule fluid than the degrees of freedom required to carry out a particle-based simulation, i.e., $N_g > 3n$. Possible exceptions (see below) are cases of fluids with soft, long-range interactions.

•*Concentrated polymer systems, especially multiphase blends and copolymer melts* appear to be best studied by FTS methods, at least if atomic-scale structure is not of interest or relevant to mesoscopic/macroscopic self-assembly behavior. We have seen in the polymer models studied here that the dimensionless chain concentration C controls the strength of fluctuation effects and thus the extent of departure from mean-field thermodynamic behavior. Since C is typically very large in concentrated solutions or melts, it is often sufficient to locate the saddle point configurations of an appropriate field theory model by invoking one of the SCFT algorithms described in this review. (It should again be emphasized that energy minimization of a particle-based model is far less useful than a saddle point computation of a corresponding field theory model.) For smaller values of C, one of the FTS sampling methods can be invoked to assess fluctuation corrections to the mean-field thermodynamics.

•*Dilute polymer solutions* are probably best studied by conventional particle-based computer simulation methods. Chemical potential field fluctuations are strong in such systems, so large deviations from the saddle point field configurations and thus mean-field behavior are expected.

•*Systems with soft, long-ranged interactions* such as electrolyte solutions, polyelectrolytes, block co-polyelectrolytes, etc. may prove to be easier to study using FTS techniques. A long-range Coulomb interaction, $v(|\mathbf{r} - \mathbf{r}'|) \sim |\mathbf{r} - \mathbf{r}'|^{-1}$, is transformed into a *short-range* interaction, $v^{-1}(|\mathbf{r} - \mathbf{r}'|) \sim \nabla^2\delta(\mathbf{r} - \mathbf{r}')$, by the Hubbard−Stratonovich transformation leading to eq 6. (Note that in this case the field $w(\mathbf{r})$ can be interpreted as a fluctuating electrostatic potential.) Thus, in FTS simulations of such systems, the cumbersome and computationally expensive techniques (such as Ewald sums) that have been developed to treat long-range interactions in particle-based simulations can be avoided. Work along these general lines is already in progress.[42,71]

•The *determination of potentials of mean force between colloidal particles* might also be conveniently addressed by FTS techniques. Colloidal suspensions with surface charges, grafted polymers, free polymers, counterions, and salts can in principle be investigated by the methods described here. Saddle point computations would provide mean-field approximations to interparticle potentials; FTS simulations could provide insights into "Casmir-like" interparticle forces caused by fluctuations in the relevant chemical and electrostatic potential fields.

•*The dynamical and rheological properties* of complex fluids are currently best addressed with particle-based simulation methods. Although some progress has been made in the context of DDFT to build time-dependent versions of mean-field theory to address the dynamics of multiphase polymers,[66,67] current formulations either neglect or oversimplify key ingredients of a fundamentally based kinetic theory of polymers, such as chain entanglements and hydrodynamic interactions. The latter, for example, are essential to properly capture drop breakup and coalescence phenomena in polymer blends. Moreover, as previously discussed, a theoretical framework is not yet available for relaxing the mean-field approximation inherent in DDFT. DPD simulations and competitive particle-based methods[96] appear to be the best options at present for studying the nonequilibrium behavior of multiphase complex fluids with

mesoscopic resolution.

A number of simulation projects in the above areas are currently under investigation in our research group and in several other computational laboratories. We hope to have a better understanding of the performance of FTS methods in such applications soon. It is also to be expected that improvements in algorithms and strategies for implementation of FTS, coupled undoubtedly with advances in computer hardware, will permit the investigation of larger, more challenging complex fluid systems. Parallel computing strategies and the introduction of advanced adaptive meshing techniques for finite element implementations of FTS appear to be especially important to pursue.

Acknowledgment. This work was partially supported by the National Science Foundation under Award Number DMR-98-70785. Acknowledgement is also made to the donors of the Petroleum Research Fund, administered by the ACS for partial support of this research. Extensive use of the UCSB-MRSEC Central Computing Facilities supported by the NSF is also gratefully acknowledged. The authors are pleased to thank H. Orland, H.-Y. Chen, M. Matsen, R. Sugar, D. Scalapino, A. Gusev, S. T. Milner, F. Schmid, J. Fraaije, and D. Duechs for helpful discussions.

References and Notes

(1) Holden, G.; Legge, N. R.; Quirk, R. P.; Schroeder, H. E., Eds. *Thermoplastic Elastomers*, 2nd ed.; Hanser/Gardner Publications: Cincinnati, OH, 1996.
(2) Kremer, K.; Muller-Plathe, F. *MRS Bull.* **2001**, *26*, 205.
(3) Hahn, O.; Delle Site, L.; Kremer, K. *Macromol. Theory Simul.* **2001**, *10*, 288.
(4) Muller, M.; Nievergelt, J.; Santos, S.; Suter, U. W. *J. Chem. Phys.* **2001**, *114*, 9764.
(5) Santos, S.; Suter, U. W.; Muller, M.; Nievergelt, J. *J. Chem. Phys.* **2001**, *114*, 9772.
(6) Balijepalli, S.; Rutledge, G. C. *Comput. Theor. Polym. Sci.* **2000**, *10*, 103.
(7) Yan, Q. L.; de Pablo, J. J. *J. Chem. Phys.* **2000**, *113*, 1276.
(8) Binder, K.; Muller, M. *Macromol. Symp.* **2000**, *149*, 1.
(9) Binder, K.; Muller, M. *Curr. Opin. Colloid Interface Sci.* **2000**, *5*, 315.
(10) Binder, K.; Paul, W. *J. Polym. Sci., Part B: Polym. Phys.* **1997**, *35*, 1.
(11) Binder, K., Ed. *Monte Carlo and Molecular Dynamics Simulations in Polymer Science*; Oxford University Press: New York, 1995.
(12) Grest, G. S.; Lacasse, M. D.; Murat, M. *MRS Bull.* **1997**, *22*, 27.
(13) Murat, M.; Grest, G. S.; Kremer, K. *Macromolecules* **1999**, *32*, 595.
(14) Groot, R. D.; Warren, P. B. *J. Chem. Phys.* **1997**, *107*, 4423.
(15) Doi, M.; Edwards, S. F. *The Theory of Polymer Dynamics*; Oxford University Press: New York, 1986.
(16) Edwards, S. F. *Proc. Phys. Soc. (London)* **1965**, *85*, 613.
(17) Helfand, E. *J. Chem. Phys.* **1975**, *62*, 999.
(18) Leibler, L. *Macromolecules* **1980**, *13*, 1602.
(19) Muthukumar, M.; Nickel, B. G. *J. Chem. Phys.* **1984**, *80*.
(20) Freed, K. *Renormalization Group Theory of Macromolecules*; Wiley: New York, 1987.
(21) Oono, Y. *Adv. Chem. Phys.* **1985**, *61*, 301.
(22) Batrouni, G. G.; Katz, G. R.; Kronfeld, A. S.; Lepage, G. P.; Svetitsky, B.; Wilson, K. G. *Phys. Rev. D* **1985**, *32*, 2736.
(23) Kennedy, A. D. *Parallel Comput.* **1999**, *25*, 1311.
(24) Ganesan, V.; Fredrickson, G. H. *Europhys. Lett.* **2001**, *55*, 814.
(25) Zienkiewicz, O. C.; Taylor, R. L. *The Finite Element Method*, 5th ed.; Butterworth-Heinemann: Boston, MA, 2000, Vol. 1.
(26) Parisi, G. *Phys. Lett. B* **1983**, *131*, 393.
(27) Lee, S. *Nucl. Phys. B* **1994**, *413*, 827.
(28) Gausterer, H. *Nucl. Phys. A* **1998**, *642*, 239.
(29) Hansen, J.-P.; McDonald, I. R. *Theory of Simple Liquids*; Academic Press: New York, 1986.
(30) Amit, D. J. *Field Theory, The Renormalization Group, and Critical Phenomena*, 2nd ed.; World Scientific: Singapore, 1984.
(31) Schoenmaker, W. J. *Phys. Rev. D* **1987**, *36*, 1859.
(32) Matsen, M. W. *Macromolecules* **1995**, *28*, 5765.
(33) Freed, K. *Adv. Chem. Phys.* **1972**, *22*, 1.
(34) Feynman, R. P.; Hibbs, A. R. *Quantum Mechanics and Path Integrals*; McGraw-Hill Book Company, New York, 1965.
(35) deGennes, P. G. *Scaling Concepts in Polymer Physics*; Cornell University Press: Ithaca, NY, 1979.
(36) Saito, N.; Takahashi, K.; Yunoki, Y. *J. Phys. Soc. Jpn.* **1967**, *22*, 219.
(37) deGennes, P. G.; Prost, J. *The Physics of Liquid Crystals*; Oxford University Press: New York, 1993.
(38) Flory, P. *Statistics of Chain Molecules*, Interscience Publishers: New York, 1969.
(39) Szleifer, I. *Curr. Opin. Colloid Interface Sci.* **1997**, *1*, 416.
(40) Matsen, M. W.; Schick, M. *Phys. Rev. Lett.* **1994**, *72*, 2660.
(41) Shi, A. C.; Noolandi, J. *Macromol. Theory Simul.* **1999**, *8*, 214.
(42) Tsonchev, S.; Coalson, R. D.; Duncan, A. *Phys. Rev. E* **1999**, *60*, 4257.
(43) Shakhnovich, E. I.; Gutin, A. M. *J. Phys. (Paris)* **1989**, *80*, 1843.
(44) Fredrickson, G. H.; Milner, S. T. *Phys. Rev. Lett.* **1991**, *67*, 835.
(45) Matsen, M. W.; Barrett, C. *J. Chem. Phys.* **1998**, *109*, 4108.
(46) Hong, K. M.; Noolandi, J. *Macromolecules* **1981**, *14*, 727.
(47) Bender, C. M.; Orszag, S. A. *Advanced Mathematical Methods for Scientists and Engineers*; McGraw-Hill Publishing Company, New York, 1978.
(48) Matsen, M. W.; Schick, M. *Curr. Opin. Colloid Interface Sci.* **1996**, *1*, 329.
(49) Schmid, F. *J. Phys.: Condens. Matter* **1998**, *10*, 8105.
(50) Press: W. H.; Flannery, B. P.; Teukolsky, S. A.; Vetterling, W. T. *Numerical Recipes*; Cambridge University Press: New York, 1988.
(51) Dennis, J. E. J.; Schnabel, R. B. *Numerical Methods for Unconstrained Optimization and Nonlinear Equations*; Prentice Hall, Inc.: New York, 1996.
(52) Janert, P. K.; Schick, M. *Macromolecules* **1997**, *30*, 3916.
(53) Matsen, M. W. *J. Chem. Phys.* **1998**, *108*, 785.
(54) Thompson, R. B.; Matsen, M. W. *J. Chem. Phys.* **2000**, *112*, 6863.
(55) Hahn, T., Ed. *International Tables for Crystallography*, 4th ed.; Kluwer Academic Publishers: Boston, MA, 1996, Vol. A.
(56) Shi, A. C.; Noolandi, J.; Desai, R. C. *Macromolecules* **1996**, *29*, 6487.
(57) Shull, K. R. *Macromolecules* **1993**, *26*, 2346.
(58) Matsen, M. W.; Bates, F. S. *Macromolecules* **1996**, *29*, 1091.
(59) Matsen, M. W. *J. Chem. Phys.* **1997**, *106*, 7781.
(60) Matsen, M. W. *J. Chem. Phys.* **1997**, *107*, 8110.
(61) Helfand, E.; Wasserman, Z. R. *Macromolecules* **1976**, *9*, 879.
(62) Whitmore, M. D.; Vavasour, J. D. *Macromolecules* **1992**, *25*, 5477.
(63) Pickett, G. T.; Balazs, A. C. *Macromol. Theory Simul.* **1998**, *7*, 249.
(64) Scheutjens, J. M. H. M.; Fleer, G. J. *J. Chem. Phys.* **1979**, *83*, 1619.
(65) Fraaije, J. *J. Chem. Phys.* **1993**, *99*, 9202.
(66) Fraaije, J.; vanVlimmeren, B. A. C.; Maurits, N. M.; Postma, M.; Evers, O. A.; Hoffmann, C.; Altevogt, P.; GoldbeckWood, G. *J. Chem. Phys.* **1997**, *106*, 4260.
(67) Maurits, N. M.; Fraaije, J. G. E. M. *J. Chem. Phys.* **1997**, *107*, 5879.
(68) Hasegawa, H.; Doi, M. *Macromolecules* **1997**, *30*, 3086.
(69) Yeung, C.; Shi, A. C. *Macromolecules* **1999**, *32*, 3637.
(70) Reister, E.; Muller, M.; Binder, K. Preprint, 2001.
(71) Tsonchev, S.; Coalson, R. D.; Duncan, A. *Phys. Rev. E* **2000**, *62*, 799.
(72) Altevogt, P.; Evers, O. A.; Fraaije, J.; Maurits, N. M.; van Vlimmeren, B. A. C. *THEOCHEM—J. Mol. Struct.* **1999**, *463*, 139.
(73) Drolet, F.; Fredrickson, G. H. *Phys. Rev. Lett.* **1999**, *83*, 4317.
(74) Drolet, F.; Fredrickson, G. H. *Macromolecules* **2001**, *34*, 5317.
(75) Sioula, S.; Hadjichristidis, N.; Thomas, E. L. *Macromolecules* **1998**, *31*, 5272.
(76) Shefelbine, T. A.; Vigild, M. E.; Matsen, M. W.; Hajduk, D. A.; Hillmyer, M. A.; Cussler, E. L.; Bates, F. S. *J. Am. Chem. Society* **1999**, *121*, 8457.
(77) Gusev, A. Unpublished work, 2001.

(78) Duechs, D.; Schmid, F. Unpublished work, 2001.
(79) Bohbot-Raviv, Y.; Wang, Z. G. *Phys. Rev. Lett.* **2000**, *85*, 3428.
(80) Fredrickson, G. H.; Helfand, E. *J. Chem. Phys.* **1987**, *87*, 697.
(81) Bates, F. S.; Maurer, W.; Lodge, T. P.; Schulz, M. F.; Matsen, M. W.; Almdal, K.; Mortensen, K. *Phys. Rev. Lett.* **1995**, *75*, 4429.
(82) Bates, F. S.; Maurer, W. W.; Lipic, P. M.; Hillmyer, M. A.; Almdal, K.; Mortensen, K.; Fredrickson, G. H.; Lodge, T. P. *Phys. Rev. Lett.* **1997**, *79*, 849.
(83) Hillmyer, M. A.; Maurer, W. W.; Lodge, T. P.; Bates, F. S.; Almdal, K. *J. Phys. Chem. B* **1999**, *103*, 4814.
(84) Laradji, M.; Shi, A. C.; Noolandi, J.; Desai, R. C. *Macromolecules* **1997**, *30*, 3242.
(85) Brazovskii, S. A. *Sov. Phys. JETP* **1975**, *41*, 85.
(86) Scalettar, R. T.; Scalapino, D. J.; Sugar, R. L. *Phys. Rev. B* **1986**, *34*, 7911.
(87) Lin, H. Q.; Hirsch, J. E. *Phys. Rev. B* **1986**, *34*, 1964.
(88) Rossky, P. J.; Doll, J. D. *J. Chem. Phys.* **1978**, *69*, 4628.
(89) Duane, S.; Kennedy, A. D.; Pendleton, B. J.; Roweth, D. *Phys. Lett. B* **1987**, *195*, 216.
(90) Alexander-Katz, A. J.; Ganesan, V.; Fredrickson, G. H. Unpublished work, 2001.
(91) Patel, D.; Ganesan, V.; Orland, H.; Fredrickson, G. H. Unpublished work, 2001.
(92) Klauder, J. R. *Phys. Rev. A* **1984**, *29*, 2036.
(93) Broseta, D.; Fredrickson, G. H. *J. Chem. Phys.* **1990**, *93*, 2927.
(94) Fredrickson, G. H.; Bates, F. S. *J. Polym. Sci., Part B: Polym. Phys.* **1997**, *35*, 2775.
(95) Duechs, D.; Ganesan, V.; Schmid, F.; Fredrickson, G. H. Unpublished work, 2001.
(96) Ahlrichs, P.; Dunweg, B. *J. Chem. Phys.* **1999**, *111*, 8225.

MA011515T